CHAPTER 17

TROPICAL CYCLONES AND CLIMATE CHANGE: A PRELIMINARY ASSESSMENT

Heather Tonkin, Gregory Holland, Christopher Landsea and Shuhua Li

17.1 Introduction: Why consider tropical cyclones and greenhouse?

Tropical cyclones, also called hurricanes and typhoons, are intense synoptic scale storms which form over warm tropical ocean regions and are the cause of major natural disasters. These storms can produce damage to coastal regions and islands through extreme wind, rain, storm surge and wave action. Increases in human settlement in tropical coastal regions is rapidly increasing global vulnerability to these tropical storms. The Pacific islands suffer extensive housing and coastal agriculture loss from tropical cyclone encounters (see, for example, Henderson-Sellers 1996). In addition tropical cyclones continue to cause considerable loss of life. A tropical cyclone in the Bay of Bengal in 1990 killed around 135 000 people. The largest damage costs come from the USA because of the high coastal infrastructure costs associated with several recent hurricanes, especially Hurricane Andrew which resulted in over US$30 billion in damage.

The characteristics of tropical cyclones vary among individual storms and between ocean regions. North Atlantic hurricanes have been linked to the El Niño-Southern Oscillation (ENSO) (Gray 1984). Although the existence and degree of an El Niño is only one of the factors affecting hurricane season statistics, the damage caused in the Florida Peninsula, the US East Coast and in the Caribbean is strongly correlated to El Niño events (cf. Chapter 6).

From hurricane data for the period 1950–1990 (Gray and Landsea 1992; Gray et al. 1993, 1994), during the 10 warmest ENSO years hurricanes have caused almost US$19 billion along the Florida peninsula and US East Coast versus US$1.5 billion during the 10 coldest ENSO years (or La Niñas). Gray et al. have also found a similar modulation in the number of intense hurricanes (those with sustained winds of at least 50 m/s): during El Niño years there were 15 intense hurricanes in the Atlantic basin whereas there were 32 during the La Niña years.

Although no detailed damage statistics are available, ENSO also effects tropical cyclone activity in the Pacific Ocean. Tropical cyclones tend to spread eastward into the central

Pacific during El Niño events, with devastating consequences for small island nations (Dong and Holland 1994).

Differences in current tropical cyclone regimes, links to complex atmosphere–ocean phenomena such as El Niño, and the difficulties of measuring the exact structure of tropical cyclones, means that the precise nature and formation process of tropical cyclones remain unclear and makes prediction of future changes in tropical cyclone characteristics very difficult (e.g. Lighthill et al. 1994). Nonetheless present vulnerability to tropical cyclones could be exacerbated by future changes in their occurrence, intensity or frequency.

The possibility of changed impacts in the future has prompted studies of greenhouse-induced changes in tropical cyclone characteristics (Emanuel 1987; Broccoli & Manabe 1990).

Concerns about possible future tropical cyclone changes can be summarised under: (i) the frequency, (ii) the area of occurrence, (iii) the mean intensity and (iv) the maximum intensity.

Two approaches have been employed to try to predict changes in tropical cyclone frequency: (1) to simply count the tropical cyclone-like vortices that appear in GCM simulations, and (2) to analyse the large-scale fields that best relate to tropical cyclone genesis (tropospheric wind shear, moist static stability, vorticity, mid-level relative humidity etc.) for changes between simulations of today's climate and in a greenhouse-warmed climate. The first approach has been attempted by Broccoli and Manabe (1990), Haarsma et al. (1993) and Bengtsson et al. (1994a, 1994b). The Haarsma et al. study suggests more tropical cyclones, the Bengtsson et al. studies suggest fewer tropical cyclones and the Broccoli and Manabe study suggests both more and fewer, depending on what type of cloudiness (either fixed or variable, respectively) is utilised.

The second approach was taken by Ryan et al. (1992) who found a substantial increase of tropical cyclones in a $2 \times CO_2$ scenario because of an increase in favourable thermodynamic parameters while the dynamic parameters changed little. However, Ryan et al. applied the Gray (1968, 1975) genesis parameter to GCM fields to obtain these findings. We have reservations about this approach, as the Gray parameter was highly tuned to fit current conditions and does not explicitly account for such thermodynamic changes as the upper-tropospheric warming in the tropics for $2 \times CO_2$. Bengtsson et al. (1994a, 1994b) found that this increased stabilisation leads to decreased frequency of cyclone type systems in a GCM. For changes in the area of occurrence, again the two methods have been utilised with mixed results. Ryan et al. (1992) suggest increases in the area of occurrence essentially because of the areal increase of oceans warmer than 26°C. We show in the following sections that the ocean temperature cut-off for cyclone formation is likely to increase in a $2 \times CO_2$ world. This is likely to result in little change in the region of cyclone development, as has been found by Bengtsson et al. (1994a, 1994b) and Haarsma et al. (1993).

Lastly, the mean intensity and maximum achievable intensity of tropical cyclones has been studied using GCM results directly by measuring the intensities of the simulated disturbances. This approach has a significant limitation in that the GCM with its coarse grid spacing is not able to capture the mesoscale structure of the inner core (and thus the true winds and

central pressure) of the storms. However GCM studies have been able to show realistic outer core circulation and thermodynamic structure of these storms. Haarsma et al. (1993) find increases in both the mean and maximum intensities in their GCM-generated storms, while Bengtsson et al. (1994a, 1994b) find no change in either the mean or maximum intensities. Broccoli and Manabe (1990) do not report how the intensities of their storms changed.

All these GCM studies suffer from the difficulty that the spatial resolution (and also probably the parameterisations) of the atmospheric models employed are much too poor to permit simulation of realistic tropical cyclones. The MECCA Analysis Team tried to evaluate the potential of exploiting 'embedded' regional climate model results in regions of tropical cyclone incidence. Careful analysis of the only MECCA simulation in such an area (Hirakuchi & Giorgi 1995) revealed that the regional model produced a worse climatology, at least in terms of the meteorological factors important in generating and sustaining tropical cyclones, than the GCM used to 'drive' it. Whether the use of regional climate models embedded within a more correct GCM simulation can provide helpful information for greenhouse scenarios is an open question.

It is clear that other means of evaluating likely future tropical cyclone activity must be sought. The following two sections deal with an attempt to use a very simple relationship between ocean temperatures and tropical cyclones, followed by the examination of a new 'downscaling' model which uses GCM results directly.

17.2 'Predicting' tropical cyclones from sea surface temperatures

While Palmen (1948) demonstrated that sea surface temperatures greater than about 26.5°C were necessary for tropical cyclone genesis to occur, it is surprising the sea surface temperature itself has nearly no relationship to mean tropical cyclone intensity (Miller 1958; Merrill 1987; Evans 1993). Sea surface temperature does, however, provide an upper bound beyond which tropical cyclones cannot become more intense (Miller 1958; Emanuel 1987; Merrill 1987; Evans 1993).

This is illustrated here by comparing the maximum intensity of tropical cyclones occurring from 1967–1992 (National Climate Data Center 1994a) as a function of climatological sea surface temperature (SST) from the Comprehensive Oceanic Atmospheric Data Set (COADS) for 1957–79 (Figures 17.1–17.3). These figures show the sea surface temperature corresponding to the location where each tropical cyclone reached its maximum intensity. The 1967–1992 period is the modern satellite era, when application of quasi-objective analysis methods, such as those of Dvorak (1975) produced the first stable cyclone data set for the majority of regions without aircraft reconnaissance (e.g. Holland 1981).

In Figure 17.1(a), showing the south west Pacific region, there are two horizontal clusters of points near 25 m s^{-1} and 33 m s^{-1}. These arise from average values of maximum wind speed for a large number of cyclones where only the Saffir-Simpson category of the storm was provided. Tropical cyclones of intensity category 2 (wind speeds greater than 16 m s^{-1} and less than 33 m s^{-1}) were presumed to have an average wind speed of 25 m s^{-1}. Category 4 storms were set to 33 m s^{-1}.

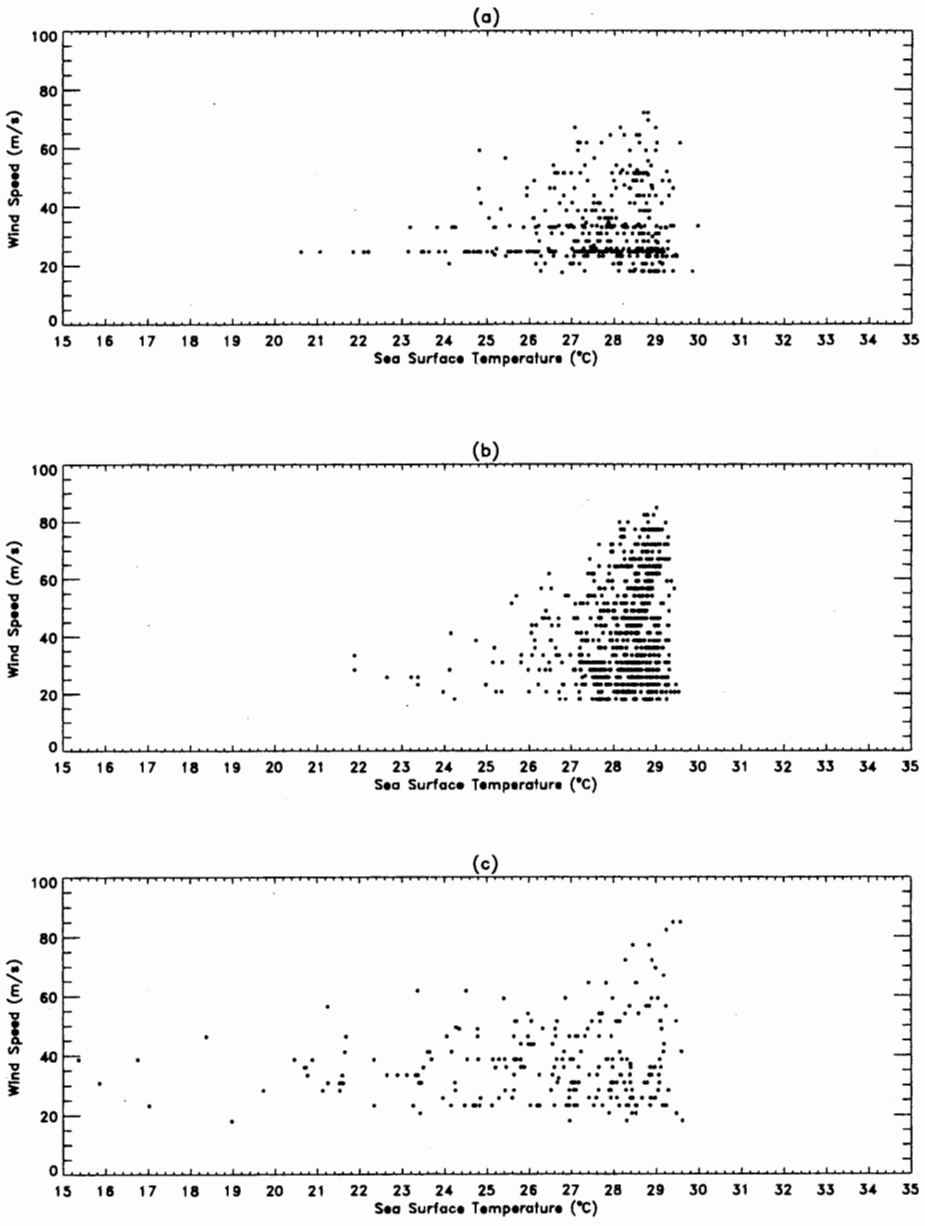

Figure 17.1 Observed maximum wind speed for individual tropical cyclones in the period 1967–1992 as a function of observed sea surface temperature for: (a) south west Pacific, (b) north west Pacific, and (c) north Atlantic.

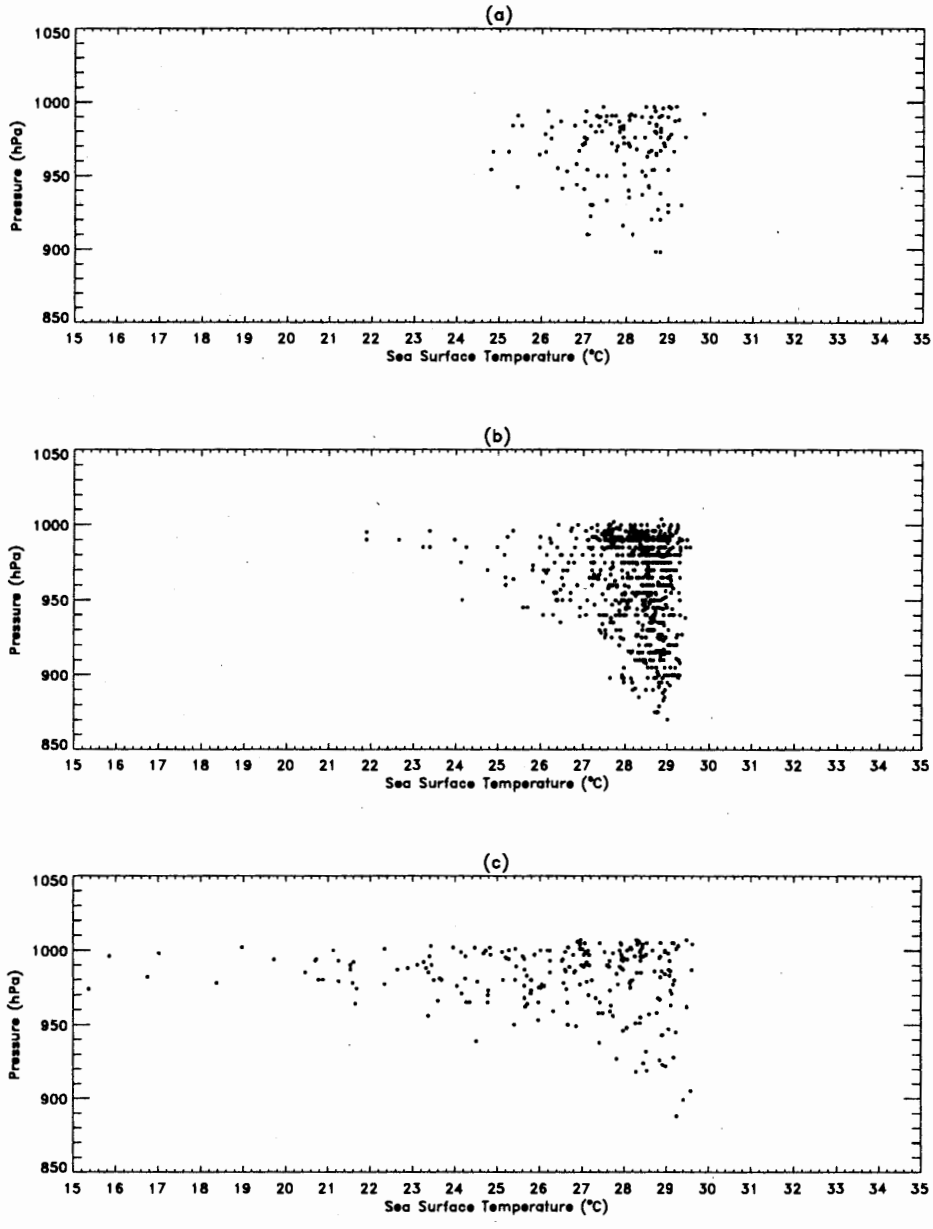

Figure 17.2 Observed minimum central pressure for individual tropical cyclones in the period 1967–1992 as a function of sea surface temperature for: (a) south west Pacific, (b) north west Pacific, and (c) north Atlantic.

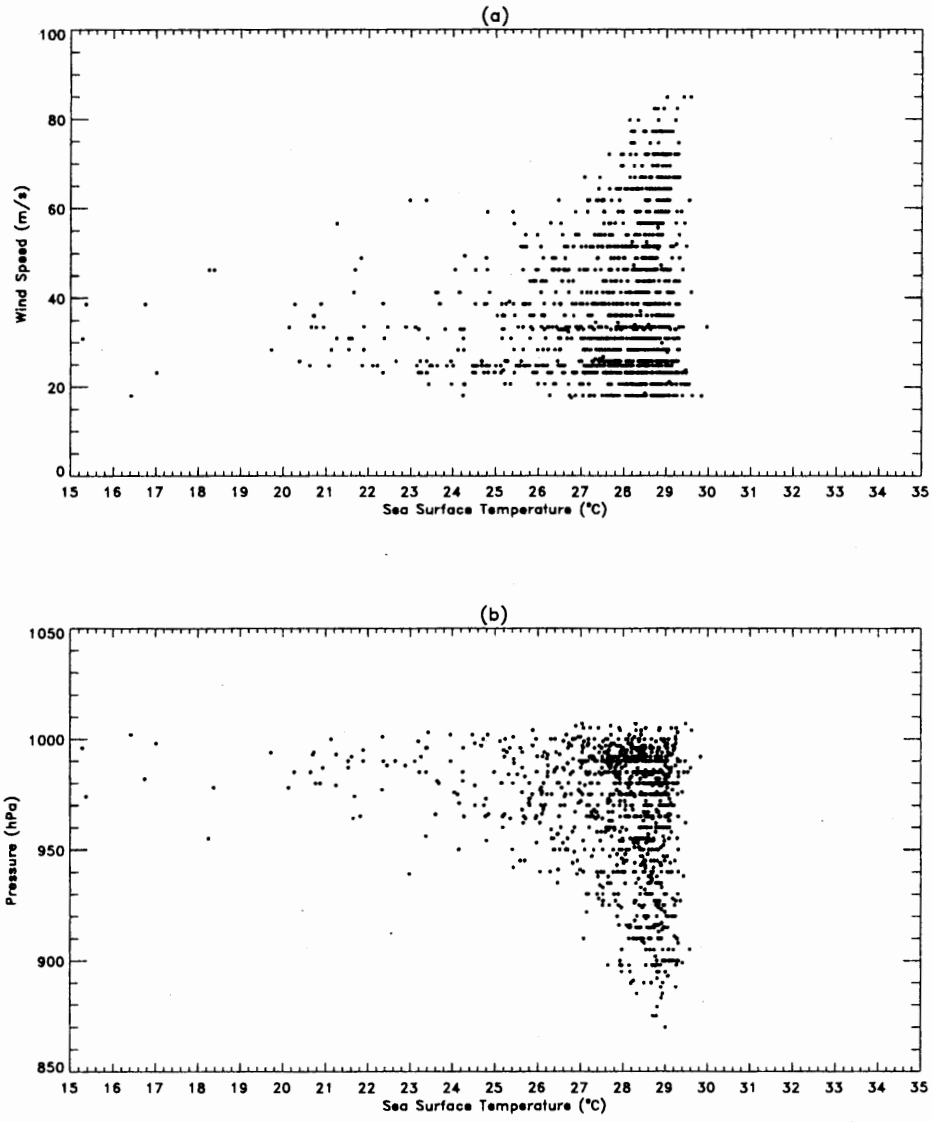

Figure 17.3 Observed maximum intensity for individual tropical cyclones in the period 1967–1992 as a function of sea surface temperature for all three ocean areas combined: (a) maximum wind speed and (b) minimum central pressure.

The results in Figures 17.1 and 17.2 illustrate an increase in maximum intensity with SST greater than 26°C (near the SST believed necessary for cyclones to form; Palmen 1948; Gray 1979). While the intensity of tropical cyclones for SST values above 26°C does not increase for the majority of storms, there appears to be a slight increase in

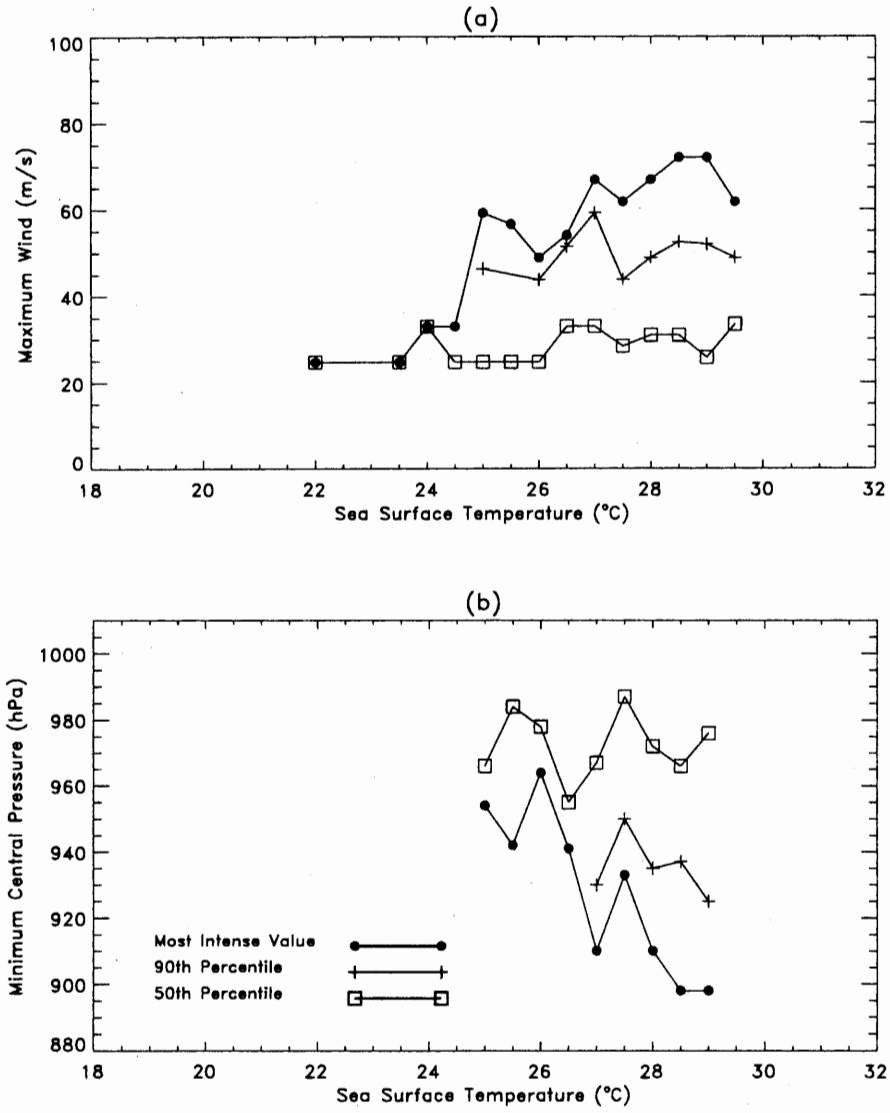

Figure 17.4 Observed most extreme, 90th and 50th percentile intensity for individual tropical cyclones in the period 1967–1992 as a function of each half degree sea surface temperature value for the south west Pacific: (a) maximum wind speed and (b) minimum central pressure.

the most intense tropical cyclones. However, above 28°C this trend is based upon a few individual cyclones. Furthermore, limitations to the accuracy of the observed data means that there is no clear trend in intensity above 28°C. Figure 17.3 combines all the available observations of tropical cyclone intensity from these three ocean regions.

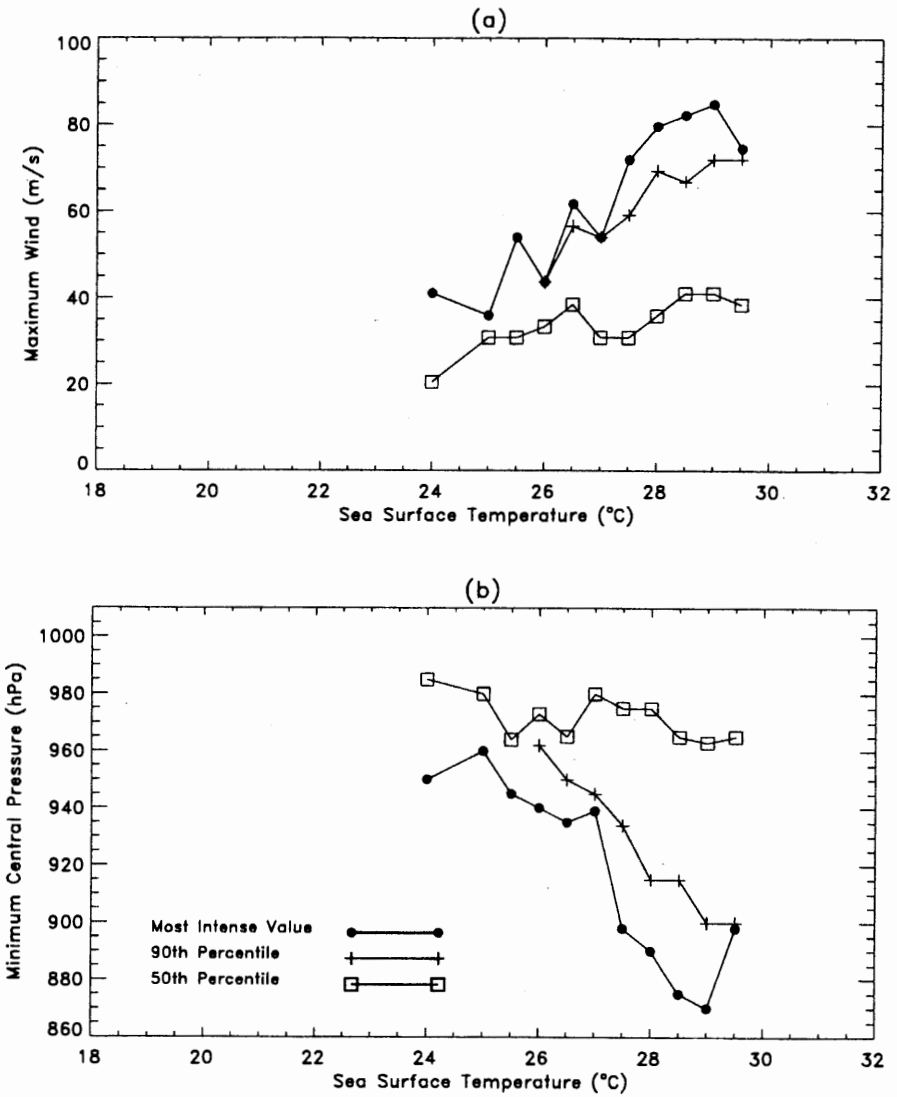

Figure 17.5 Observed most extreme, 90th and 50th percentile intensity for individual tropical cyclones in the period 1967–1992 as a function of each half degree sea surface temperature value for the north west Pacific: (a) maximum wind speed and (b) minimum central pressure.

Limitations on the accuracy of these graphs include: (i) the maximum intensity often occurs over a range of locations, as the tropical cyclone may have retained a maximum intensity level for a number of hours and so the location of maximum intensity are average values; (ii) measurements of tropical cyclone intensity are not very accurate — especially

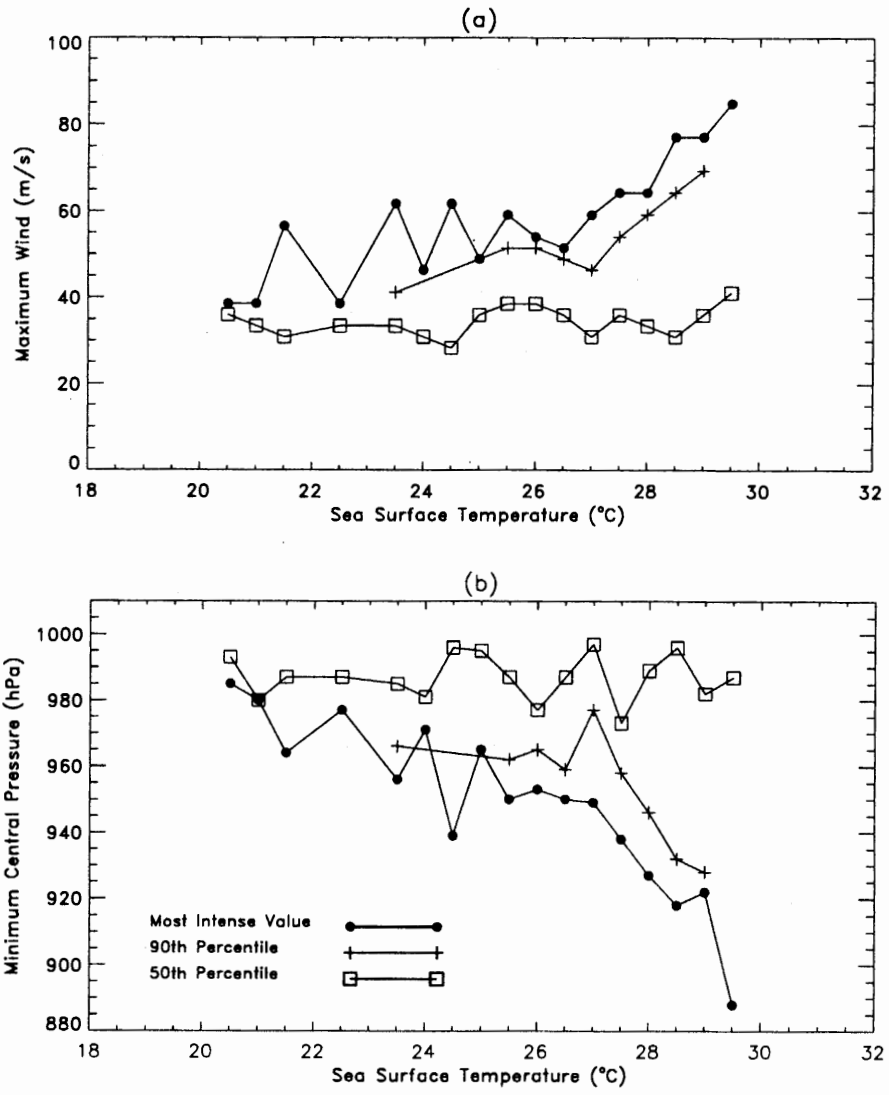

Figure 17.6 Observed most extreme 90th and 50th percentile for individual tropical cyclones in the period 1967–1992 as a function of each half degree sea surface temperature value for the north Atlantic: (a) maximum wind speed and (b) minimum central pressure.

if satellite pictures are used to infer (not measure directly) tropical cyclone intensity, as is done in the south west Pacific and in the north west Pacific since 1987; (iii) COADS is comprised of monthly averaged ship observations of SST within a 2 × 2 degree box, time and space scales smaller than this are smoothed out; and (iv) no account is taken of local

SST cooling arising from the direct interaction between the tropical cyclone and the ocean (Shay et al. 1992).

However these results compare quite well with Evans (1993) who produced similar scatter plots using data from 1967–1986 from the Constructed World Wide Tropical Cyclone Data Set.

Figures 17.4 to 17.6 are plots of observed maximum intensity against SST for the south west Pacific, north west Pacific and north Atlantic ocean regions. COADS data was used to find the SST value for the locations where each tropical cyclone reached maximum intensity. Maximum intensity data is taken from National Climate Data Center (NCDC) (1994a). These plots represent the most intense, 90th percentile and 50th percentile storm which occurred at each half-degree ocean temperature from 18°C to 32°C. Each ocean region is represented by two sets of plots where maximum intensity values were taken as either the maximum wind speed or minimum central storm pressure. There are slight variations between the cyclones selected by each of the processes because cyclones of the same minimum central pressure will not necessarily have the same maximum wind speed.

In the Australian region values of minimum pressure were not generally provided in the NCDC data set until 1980, and this explains the small range of SST values corresponding to maximum tropical cyclone intensity in Figure 17.4(b) compared to Figure 17.4(a). Therefore, in the south west Pacific (Australian) region it is more useful to examine the trend in maximum intensity with SST by considering wind speed values. Figure 17.4(a) shows a clear increase in maximum intensity with SST up to 29°C. However the increase in maximum intensity appears to reduce as SSTs increase. Potential reasons for this are presented later. Beyond 29°C, the number of observations for each half degree SST value decreases, which means the recorded maximum intensity values are unlikely to be the most intense possible for these SST values.

Figure 17.4(a) might be divided into two or even three segments: SSTs below 25°C have low maximum intensity (less than 35 m s^{-1}); between 25°C and 26.5°C there is an intermediate intensity range where maximum intensity are from 50 m s^{-1} to 60 m s^{-1}. For SST values greater than 26.5°C cyclone intensity appears to be above 60 m s^{-1}. The cluster, however, may be partly due to the NCDC data set which frequently only supplied the cyclone intensity category and so many hurricane strength storms were given the intensity value of 33.0 m s^{-1} which is the minimum wind speed for hurricane strength.

Figures 17.5(a) and 17.5(b) show maximum intensity trends for the north west Pacific region where 604 cyclones occurred from 1967–92. There is a clear increase in tropical cyclone intensity with increasing SST. There appears to be a cluster of points in Figure 17.5(b), with SST values less than 27.5°C maintaining cyclones of greater than 940 hPa. For SSTs above 27°C, the maximum intensity ranges from 870–900 hPa. This cluster of points is not as apparent in Figure 17.5(a), although low intensity storms may be said to exist at SST values below 25°C, medium intensity storms between 25°C and 27°C, while strong storms occur where SSTs exceed 27°C.

North Atlantic cyclones reach maximum intensity over colder ocean regions than in the south or north west Pacific regions. In Figure 17.6(b) there is a cluster of maximum intensity

points below SST values of 23°C where intensity values range from 960–990 hPa. From 22.5°C to 27°C the tropical cyclone intensity ranges from 940–970 hPa, and beyond 27°C maximum intensity increases to 890 hPa. The cluster of maximum intensity values exists for wind speed maximum intensity values, (Figure 17.6(a)) though they are less clearly defined. Least intense storms exist below 23.5°C. Medium intensity tropical cyclones range from 23.5°C–26.5°C. Above 26.5°C storm intensity increases, and appears to level out between 28.5°C and 29°C, before increasing again at 29.5°C. Figure 17.7 illustrates the trend in maximum intensity for increasing SSTs for all three ocean regions combined. Significant features of Figure 17.7(b) include the increase of maximum intensity with SST and clusters of points below SSTs of 23°C (above 960 hPa), between 23°C and 26.5°C (940–960 hPa) and from 26.5°C (870–910 hPa). Figure 17.7(a) may follow the same general clustering of points, however this is less clearly defined. Examining the scatter graphs from the three regions combined, there appears to be three main levels of maximum tropical cyclone intensity determined by a region's SST. These are least intense storms where central pressure is greater than 960 hPa, intermediate intensity where maximum intensity is ~940 hPa and most intense storms between 870–910 hPa.

The observed relationships between SST and maximum intensity might form the basis of a prediction method if there was: (a) a better correlation and (b) greater skill in modelling ocean surface temperatures (see, for example, Chapter 7). However such analysis assumes that the SST/maximum intensity relationship for current climate is maintained in a $2 \times CO_2$ climate. In the following section, we establish a predictive model for tropical cyclone maximum intensity which draws on a larger range of GCM fields.

17.3 Downscaling models of tropical cyclones

In common with most other areas of impact assessment, those concerned with tropical cyclone simulations have sought means by which coarse-resolution global circulation models can be utilised to estimate fine-resolution characteristics such as tropical cyclone intensity. One such approach is to develop a set of physical relationships between the thermodynamic state of the atmosphere and ocean, and the maximum potential intensity (MPI) of tropical cyclones.

The MPI achievable by a tropical cyclone was first assessed by Kleinschmidt (1951) and Miller (1958) who extended and quantified earlier work by Palman (1948), Riehl (1954) and Abdullah (1954). Miller derived a relationship between MPI and SST by assuming saturated moist ascent in the eye wall clouds to define a cloud-top from which air subsided in the eye. The subsiding air warms from dry adiabatic compression and Miller included a parameterised cooling from entrainment of eye-wall cloud into the eye. The method predicted increasing MPI with SST though the MPI/SST relationship devised was not uniquely defined. Miller did not include the important feedback between the ocean and tropical cyclone that occurs (Byers 1944; Riehl 1954; Malkus & Riehl 1960). This feedback arises through the dependence of equivalent potential temperature on pressure as well as temperature and humidity. As the surface pressure falls, whilst the temperature and humidity

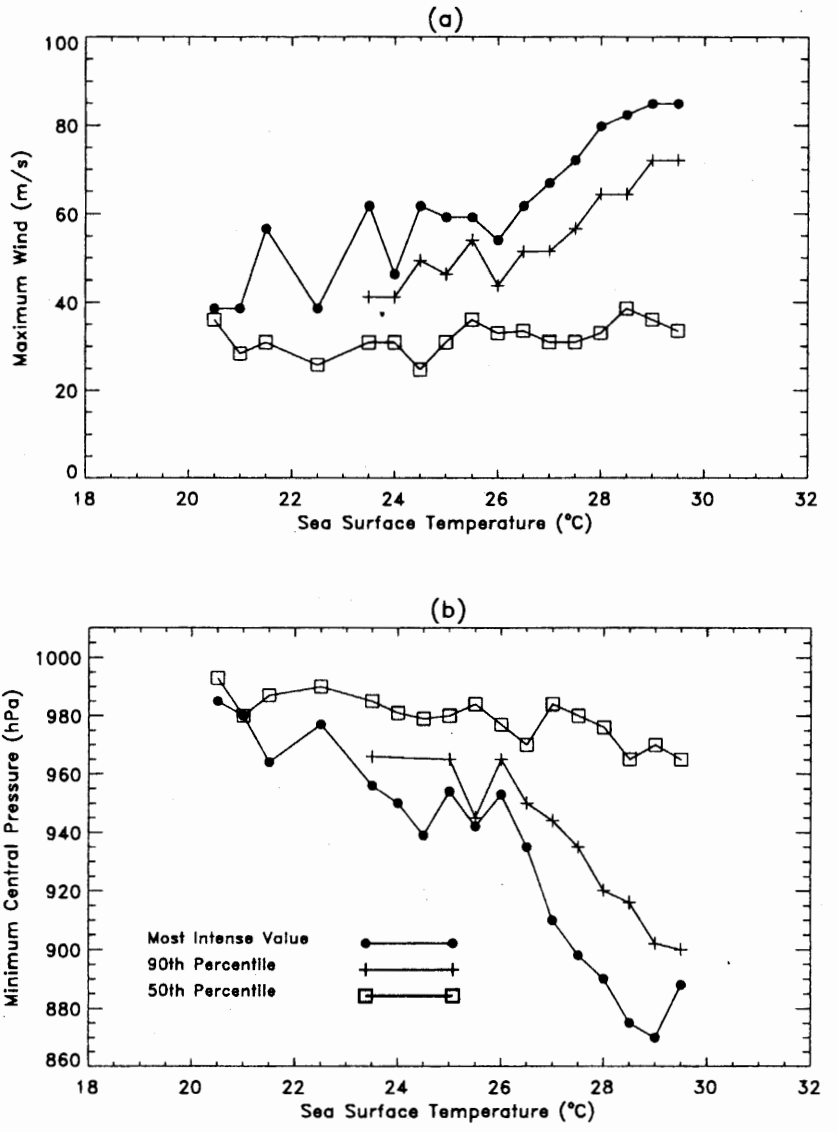

Figure 17.7 Observed most extreme, 90th and 50th percentile intensity for individual tropical cyclones in the period 1967–1992 as a function of each half degree sea surface temperature value for all three ocean areas combined: (a) maximum wind speed and (b) minimum central pressure.

remain constant, the equivalent potential temperature increases. Thus the ocean is able to release additional energy to the atmosphere with decreasing central pressure. A positive feedback cycle thus results to support the development of intense tropical cyclones (see Holland 1996 for a detailed discussion).

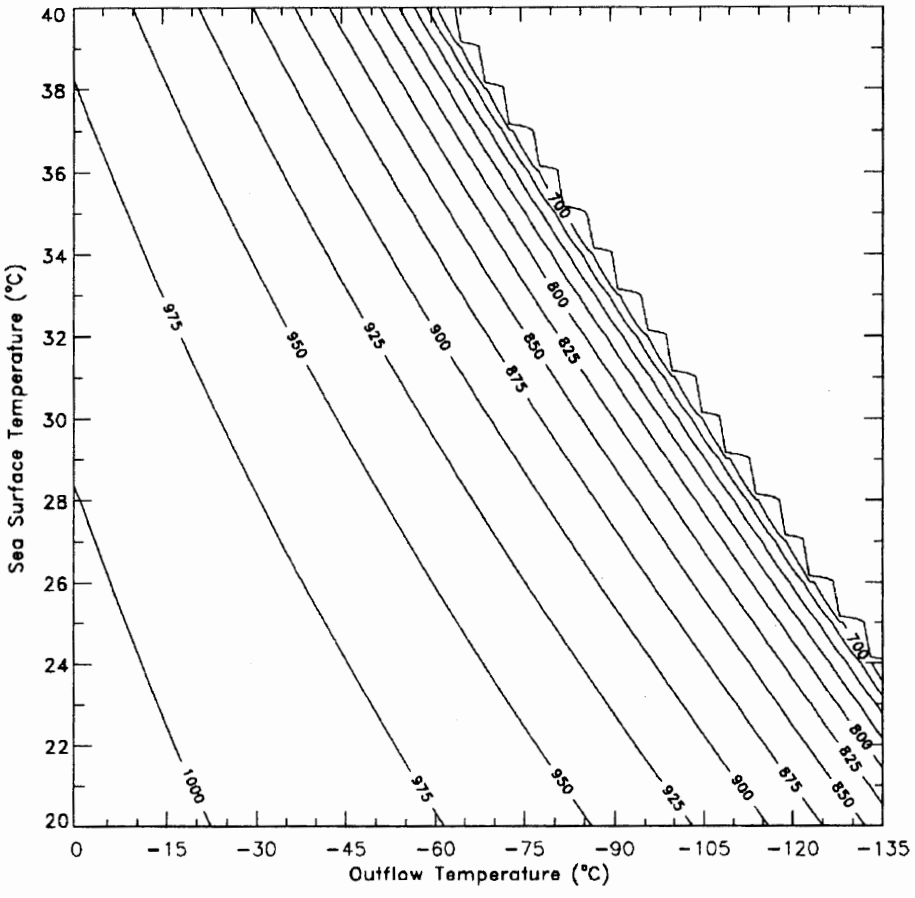

Figure 17.8 Relationship between sea surface temperature, tropical cyclone outflow layer temperature and estimated maximum potential tropical cyclone intensity (Emanuel Model). RH of 75%, ambient surface pressure of 1015 hPa, latitude 20°N, tropical cyclone radius of 500 km.

Emanuel (1987) applied one such thermodynamic model to the Goddard Institute for Space Studies (GISS) GCM and found that the MPI increased markedly in a $2 \times CO_2$ environment. Emanuel's model is based on a conceptual view of a tropical cyclone as a Carnot heat engine. The model assumes a steady state balance where angular momentum, total entropy and total water are conserved and the atmosphere is taken to be neutral to slantwise moist convection. The cyclone intensifies through a feedback mechanism: evaporation from the sea surface to the atmosphere increases as wind speeds increase in response to greater pressure gradient forces arising from falling central pressure values. Decreasing central pressure is due to increasing latent heat release in

the cyclone core as converging wind speed increases. The model predicts maximum tropical cyclone intensity will rise with rising SST and with colder (higher) outflow conditions.

Emanuel used this method to derive a relationship between SST, outflow temperature and MPI (Figure 17.8). This relationship predicts an increase of MPI for SST increases, similar to the observations in Figures 17.4–17.7 however the predicted increase tends to be stronger than that which is observed, and an exponential increase at higher SST is not sustained by the observed intensity which shows a decrease in the rate of intensity change.

There are difficulties with relation to the highly asymmetric outflow of a real tropical cyclone to Emanuel's axisymmetric outflow temperature. Emanuel includes no eye processes and assumes a saturated cloud-filled core. Further, highly complex ocean interactions occurring under high wind conditions (Pudov & Holland 1994; Fairall et al. 1995) are neglected. As shown by Holland (1995) the major sensitivity is to the assumed values of relative humidity in the core region and the environment.

Holland (1995) has developed an approach to the thermodynamic prediction of MPI which contains both the ocean feedback and an explicit eye. In this approach the ocean feedback occurs under the eye wall where the relative humidity is assumed to be 90%. The eye is parameterised in a similar fashion to Miller (1958). This approach requires no estimate of the outflow temperature and explicitly derives the cloud detrainment level which defines the eye subsidence and the height of eye-wall warming. A direct relationship between SST and MPI is derived by using series of monthly-mean soundings in tropical cyclone ocean basins.

This approach agrees closely with observed maximum intensity and also explicitly predicts that intense tropical cyclones will not develop for SSTs below 26°C in the current climate. Holland also shows that for SSTs greater than 26°C the relationship is quite stable across ocean basins.

Limitations of Holland's approach include the assumption of a vertical eye-wall, lack of inclusion of spray effects in high wind conditions, lack of entrainment into the eye-wall and the assumption of 90% relative humidity (RH) at the surface under the eye wall. Holland argues that the lack of a sloping eye-wall is not a major limitation. The results are quite sensitive to the RH assumption, but less so than that in Emanuel's approach.

Figures 17.9(a) and 17.9(b) show MPI from the Holland and Emanuel 'downscaling' models for eleven radiosonde station locations in coastal north Australia (Figure 17.10).

For the Holland model, observational data include radiosonde retrievals of monthly averaged air temperatures from 850 hPa to 100 hPa and average monthly surface pressure data (Maher & Lee 1977). Seventeen vertical temperature and pressure levels were used to calculate the MPI, archived radiosonde data provided ten levels and the remainder were obtained by interpolation. Relative humidity in the tropical cyclone eye wall was taken to be 90%. Surface air temperatures were calculated as one degree less than SST values of the nearest 2×2 degree ocean grid to each radiosonde station. The SST data was taken from COADS (Slutz et al. 1985) consisting of monthly averaged values from 1951–1979. For the Emanuel model, local temperature profiles used to calculate the tropical cyclone outflow temperature

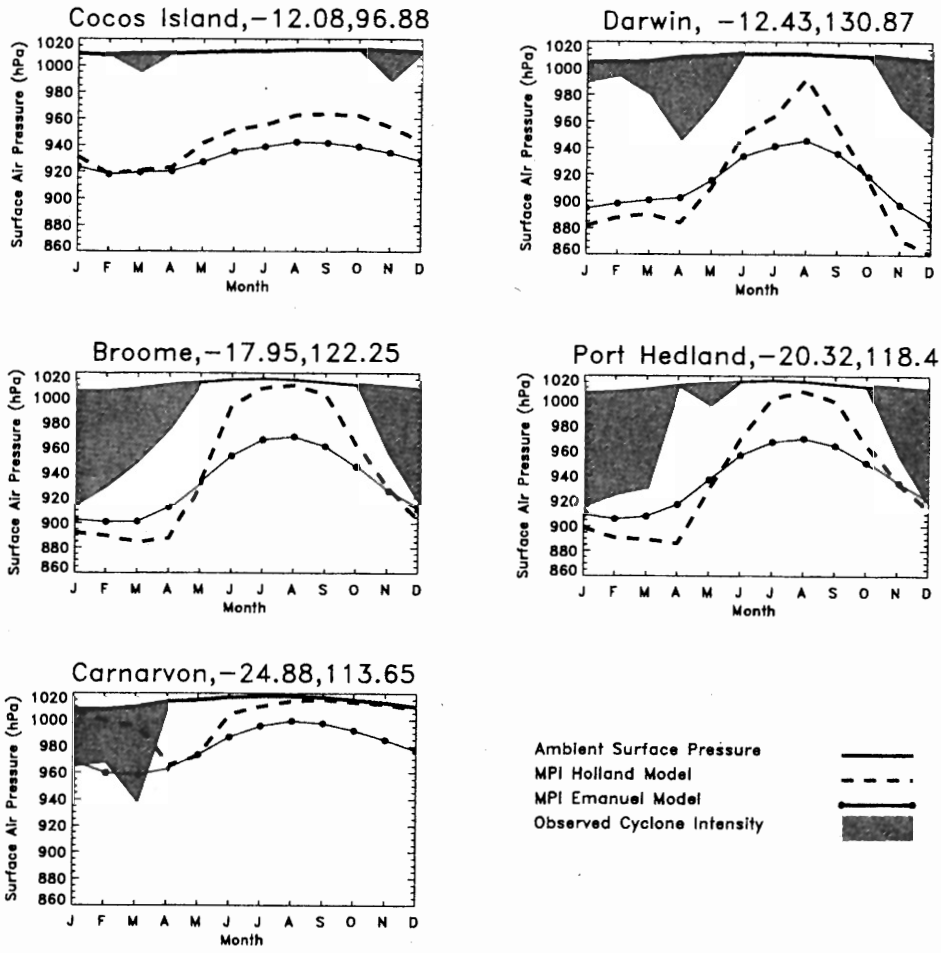

Figure 17.9(a) Simulated (Holland and Emanuel models) and observed maximum potential intensity for the western Australian region.

and ambient surface pressure were also taken from Maher and Lee (1977). Ambient relative humidity was set at 80% and surface relative humidity at the storm centre was set to 100%. Surface temperatures were taken as the SST value of the nearest 2×2 degree ocean grid to each radiosonde station (COADS). Observed cyclone intensity values were collected from the Tropical and Extra Tropical Cyclone Track CD (National Climate Data Center 1994a) and consist of the lowest central pressure within 5 degrees latitude of each station from 1967–92. Only storms of at least tropical cyclone intensity (wind speed greater than 17.5 m s^{-1}) were used.

Care needs to be taken with the use of soundings adjacent to a major landmass as representative of the oceanic regime in which tropical cyclones form. The soundings may

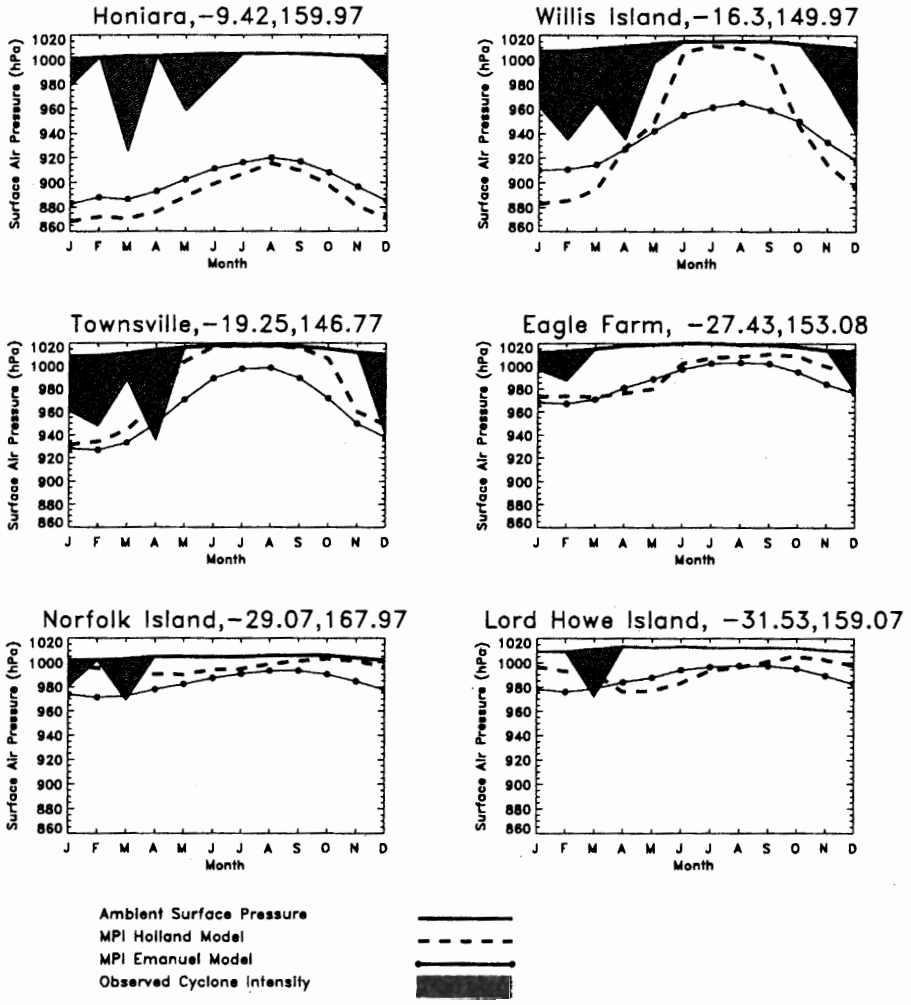

Figure 17.9(b) Simulated (Holland and Emanuel models) and observed maximum potential intensity for the eastern Australian region.

be defined more by radiative equilibrium over the land mass, which contains extensive areas of hot desert country. This is more of a problem for the Holland model, as the Emanuel approach assumes an 80% RH in the environment (which can be very dry near the land). As a general rule, use of such soundings in the Holland model will underestimate the capacity of the oceanic regime to generate intense tropical cyclones. At low latitude stations such as Broome, Port Hedland, Willis Island and Townsville, the Holland model predicts

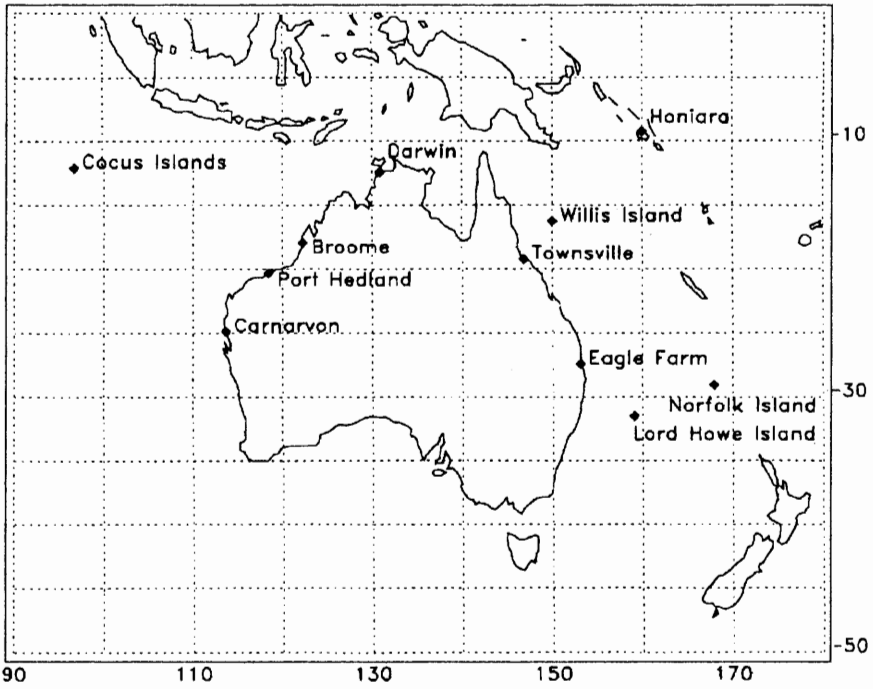

Figure 17.10 Australian region station locations for Figures 17.9(a) and 17.9(b).

definite MPI differences between summer and winter months, suggesting a well-defined tropical cyclone season exists at these locations. The exception to this is Honiara, Cocus Island and to a lesser extent Darwin, which show potential tropical cyclone activity through most of the year. At these latitudes, the Emanuel model predicts tropical cyclones throughout the year. As well, MPI estimated from the Emanuel model has less monthly variability of MPI than the Holland model.

At mid-latitude locations, both models show a potential for weak tropical cyclones within a short tropical cyclone season. At Carnarvon, Norfolk Island and Lord Howe Island, the Holland model appears to slightly underestimate tropical cyclone intensity. The observed intensities at these locations may be higher than the available thermodynamic energy would permit because tropical cyclones which move poleward may have intensities corresponding to slightly warmer conditions.

In general, the model results correspond reasonably well with observations in the south west Pacific. However, the short observational period means that there are few observed tropical cyclones at each location with which to provide an accurate comparison of model results.

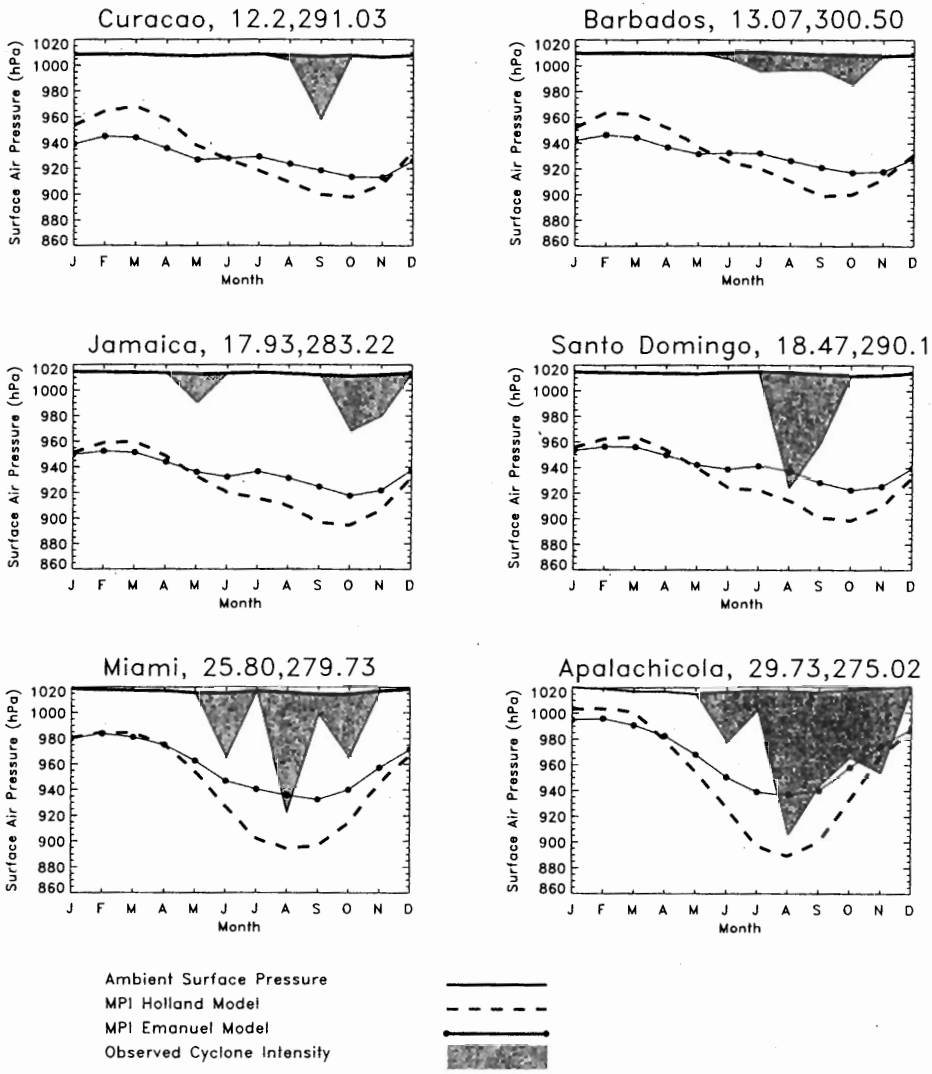

Figure 17.11(a) Simulated (Holland and Emanuel models) and observed maximum potential intensity for the north Atlantic region.

Figures 17.11(a) and 17.11(b) contain estimated MPI values for the Holland and Emanuel 'downscaling' models for nine radiosonde stations in the north Atlantic Ocean region (Figure 17.12). Data sources for these calculations were as for the Australian region except radiosonde data retrievals of monthly averaged air temperature and monthly averaged surface pressure were from the NCDC (1994b) and extended to 30 hPa. For the Emanuel model in this region MPI calculations used temperature values up to 30 hPa.

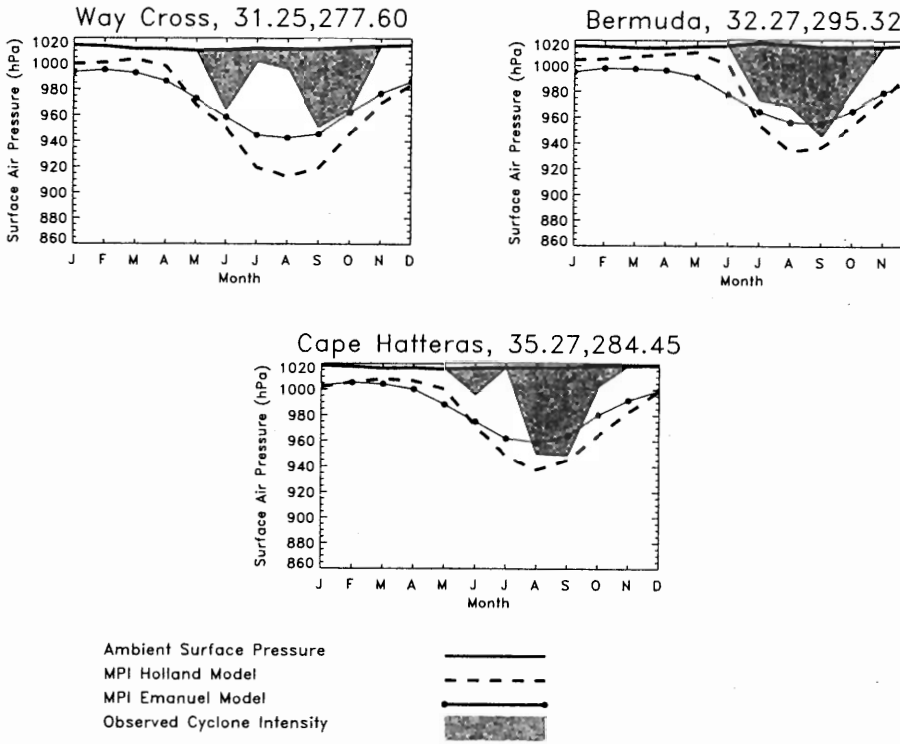

Figure 17.11(b) Simulated (Holland and Emanuel models) and observed maximum potential intensity for the north Atlantic region.

For low latitude stations, both models predict tropical cyclones all year round, although the Holland model predicts decreased intensity in colder months, and the Holland model predicts more intense tropical cyclones than the Emanuel model during the tropical cyclone season.

At low latitude locations the observed intensity appears significantly less than the MPI estimated from both models. Possible reasons for this may be the small number of observed cyclones near these stations over the last 30 years. A more likely explanation, however, is that the dynamics of cyclone development generally require time scales of days to move from formation to maximum intensity. During this time, cyclones typically move poleward at several meters per second, so that they do not generally remain in the deep tropics for sufficient time to develop to maximum intensity.

Figures 17.11(a) and 17.11(b) show considerable seasonality, at higher latitude locations such as Miami, Apalachicola, Way Cross, Bermuda and Cape Hatteras where cyclones are mostly predicted during the tropical cyclone season (between May and October) for both models. For these stations, the Holland model predictions correspond well with observations, and the Emanuel model estimates appear underestimated at some locations.

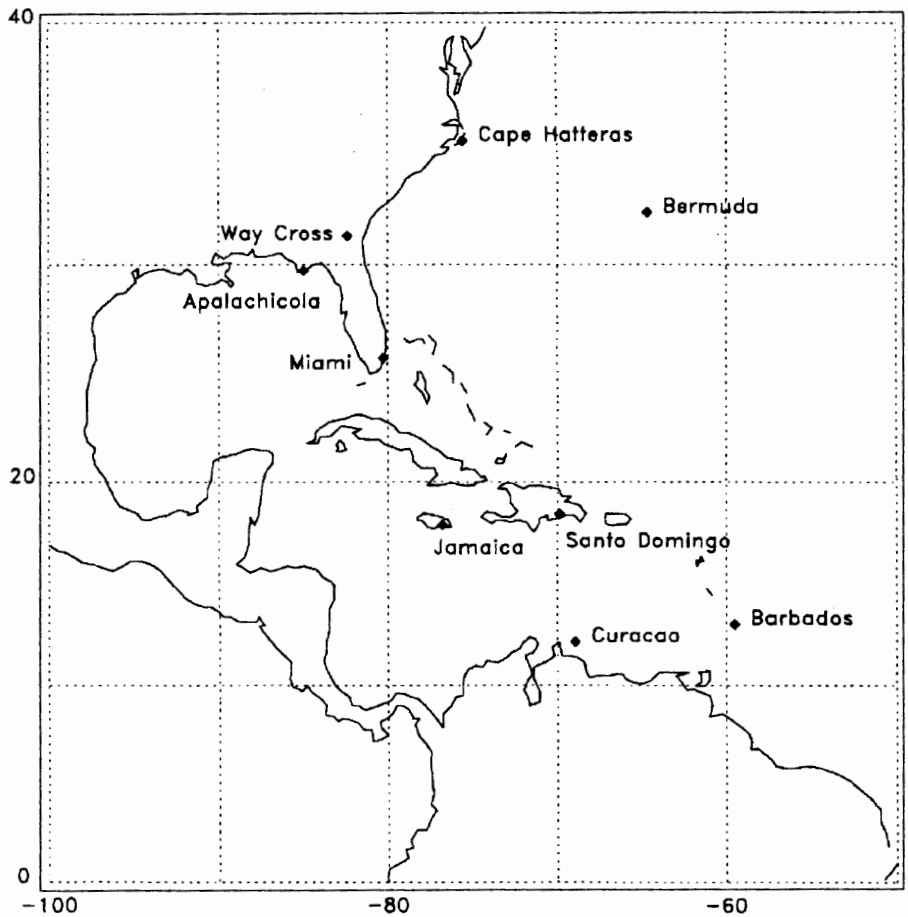

Figure 17.12 North Atlantic region station locations for Figures 17.11(a) and 17.11(b).

Figures 17.13(a) and 17.13(b) show MPI from both models for the north west Pacific region (Figure 17.14). Data sources and calculation methods are the same as those used for the north Atlantic region.

For low latitude stations of Palau, Kwajalein and Guam, tropical cyclones are predicted all year for both models. This appears reasonable at Guam, where tropical cyclones are observed throughout the year. Palau and Kwajalein are located close to the equator in a region of relatively low planetary vorticity, which is considered unfavourable for tropical cyclone development (Gray 1968). Tropical cyclones in this region are typically in the early stages of development, and tend to move towards the north west in the easterly air flow, reaching maximum intensity at higher latitudes. This may explain the lack of observed tropical cyclone at these stations.

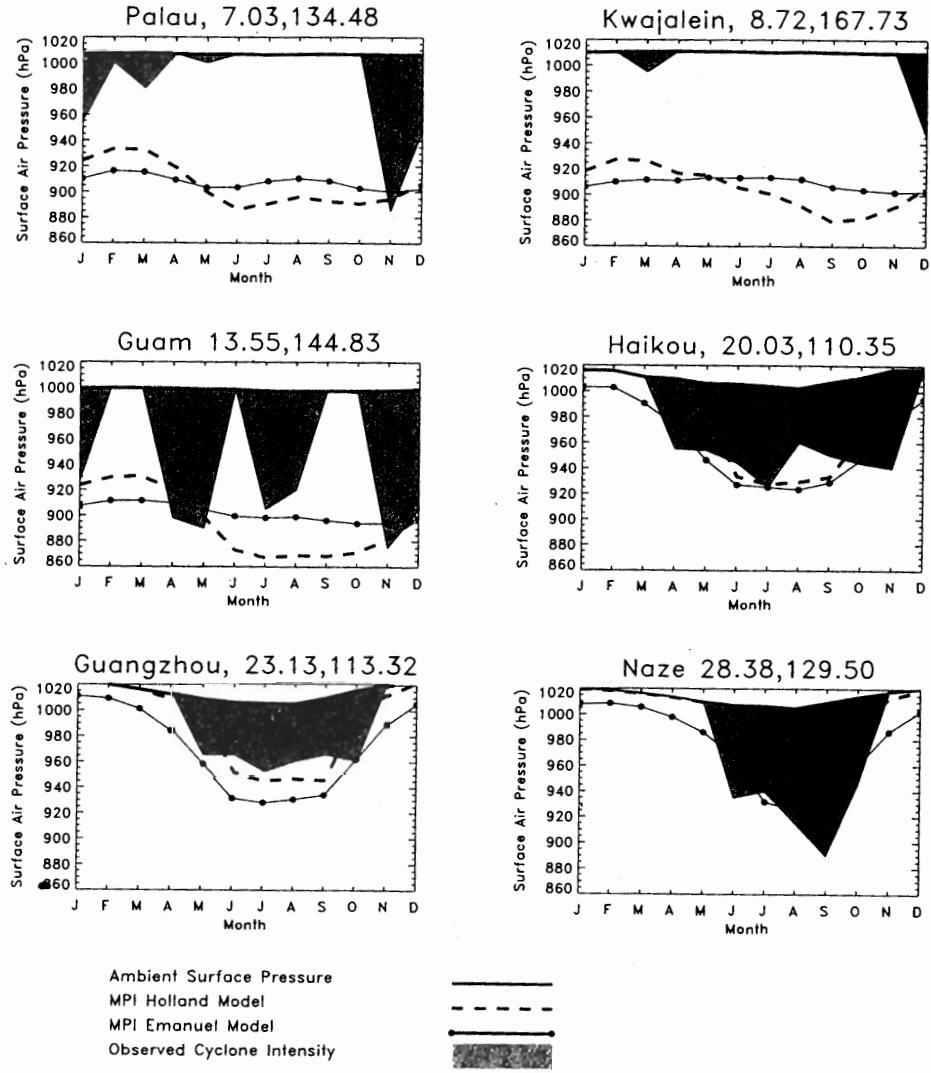

Figure 17.13(a) Simulated (Holland and Emanuel models) and observed maximum potential intensity for the north west Pacific region.

In this ocean region the Emanuel model is slightly more intense than the Holland model at latitudes above 20°N. For Haikou, Guangzhou and Naze, both models appear to underestimate MPI. For high latitude stations, predicted MPI from both models is much reduced and limited to a short cyclone season. At Tateno, the effect of advection of weakening storms from lower latitudes is clearly seen.

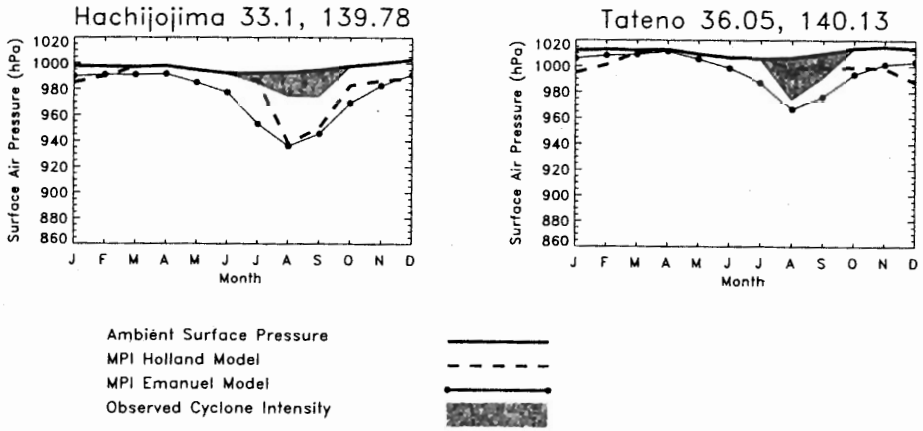

Figure 17.13(b) Simulated (Holland and Emanuel models) and observed maximum potential intensity for the north west Pacific region.

In general, the Holland and Emanuel models predict similar tropical cyclone intensity which corresponds reasonably with observations, the major differences being a larger seasonal variability of MPI from the Holland model generally, and in particular at low latitudes.

Figure 17.15 shows the relationship between observed and predicted maximum tropical cyclone intensity, together with the 50th percentile of observed intensities for comparison. Significant features include the near linear increase of maximum intensity for SSTs greater than 26°C for both models and observations. The Holland model captures actual intensities more accurately than does Emanuel's model, though both provide generally good indications of the maximum cyclone intensity/SST relationship. As discussed by Holland (1996), SST is a dominant factor in determining the radiative/convective equilibrium of the overlying atmosphere and thus provides a good, first order proxy to the full thermodynamics.

Results from the Holland and Emanuel models in the south west Pacific, north Atlantic and north west Pacific regions indicate the Holland model captures tropical cyclone seasonality quite well. MPI values from the models appear reasonable (within the range of intensities experienced in each region) although MPI values do not always closely match observed intensities.

While both the Emanuel (1991) and Holland (1996) thermodynamic methods of predicting MPI have significant limitations, they show agreement with observations and provide an objective method of interpreting GCM predictions of $2 \times CO_2$ changes to climate for potential tropical cyclone changes. It is especially important to note that the use of SSTs alone is not a valid approach and the models must be applied to the full soundings as SST changes arising from anthropogenic climate change are associated with different mechanisms and much different overlying atmospheric structures than are changes associated with seasonal or transitory changes in current climate.

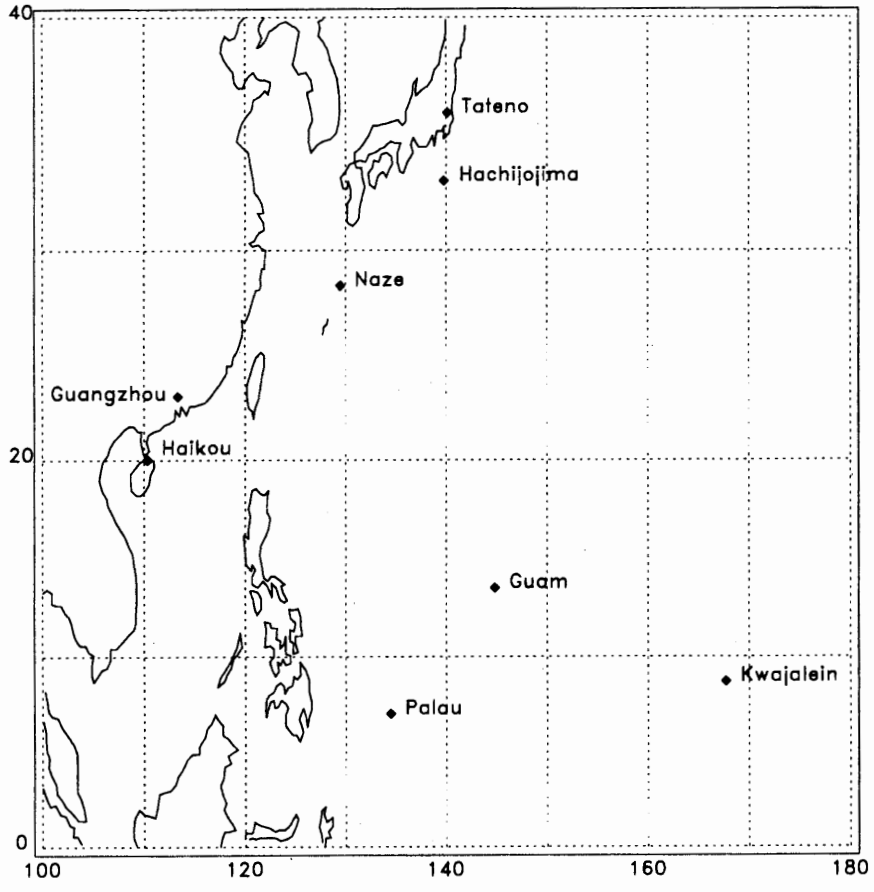

Figure 17.14 North west Pacific locations for Figures 17.13(a) and 17.13(b).

Both of these models can be used as downscaling tools since the problem with using GCM models to explicitly capture the structure of tropical cyclones is bypassed by these thermodynamic models. In addition using information averaged over GCM grid areas is less problematic than other applications, as parameters such as SST do not vary greatly in the tropics. Such tools have the potential to estimate information about future tropical cyclone intensity potential over GCM grid size areas.

Overall, however, the Holland model performs better than the Emanuel model in the three regions examined. The predictions are good enough to justify the next stage in this preliminary analysis.

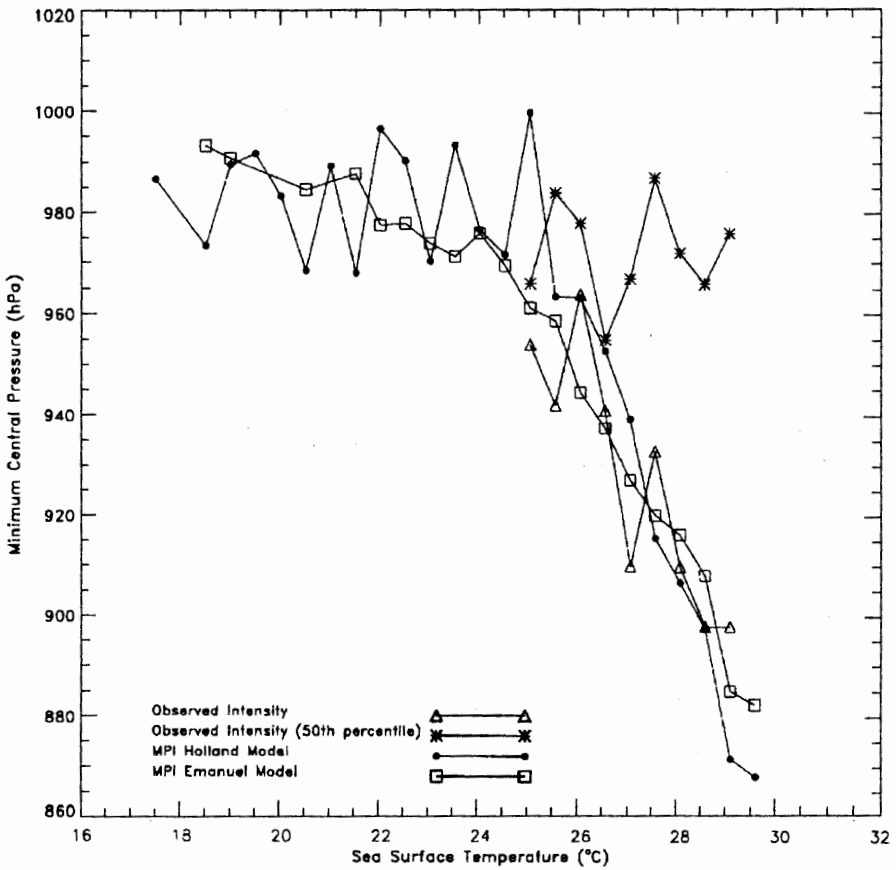

Figure 17.15 Maximum and 50th percentile observed and maximum predicted potential intensity (Holland and Emanuel models) for tropical cyclones as a function of sea surface temperature for the south west Pacific. (Only where three or more observed cyclones occurred at a given temperature were the points included in the profiles.)

17.4 Estimations of tropical cyclone changes from selected MECCA GCM simulations

The following analysis examines both the capacity for GCMs to reproduce current climatic conditions for tropical cyclones and the predicted changes that may occur. The analysis is focussed on application of the Holland model to six climate model simulations over the western North Pacific in August, the month and location of maximum global MPI. The data consist of mean fields from the following selection of the MECCA Phase 1 experiments (e.g. Henderson-Sellers et al. 1995).

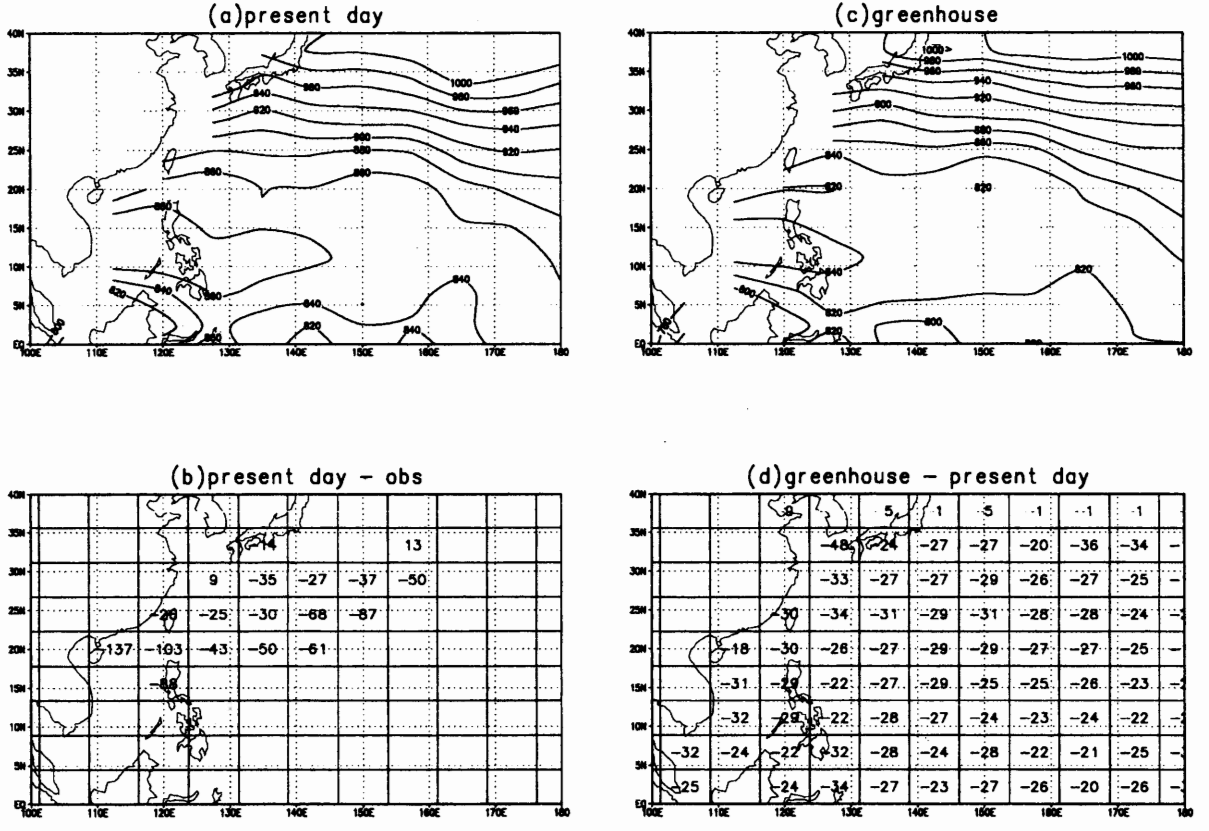

Figure 17.16 (a) Simulated maximum potential intensity (Holland model) for tropical cyclones in the north west Pacific from present-day climate simulations with the CCM1-OZ for August; (b) differences (GCM simulations — observed) at GCM grid locations; (c) simulations of maximum potential intensity for a greenhouse-warmed climate; (d) differences ($2 \times CO_2$ GCM simulations — current GCM simulations).

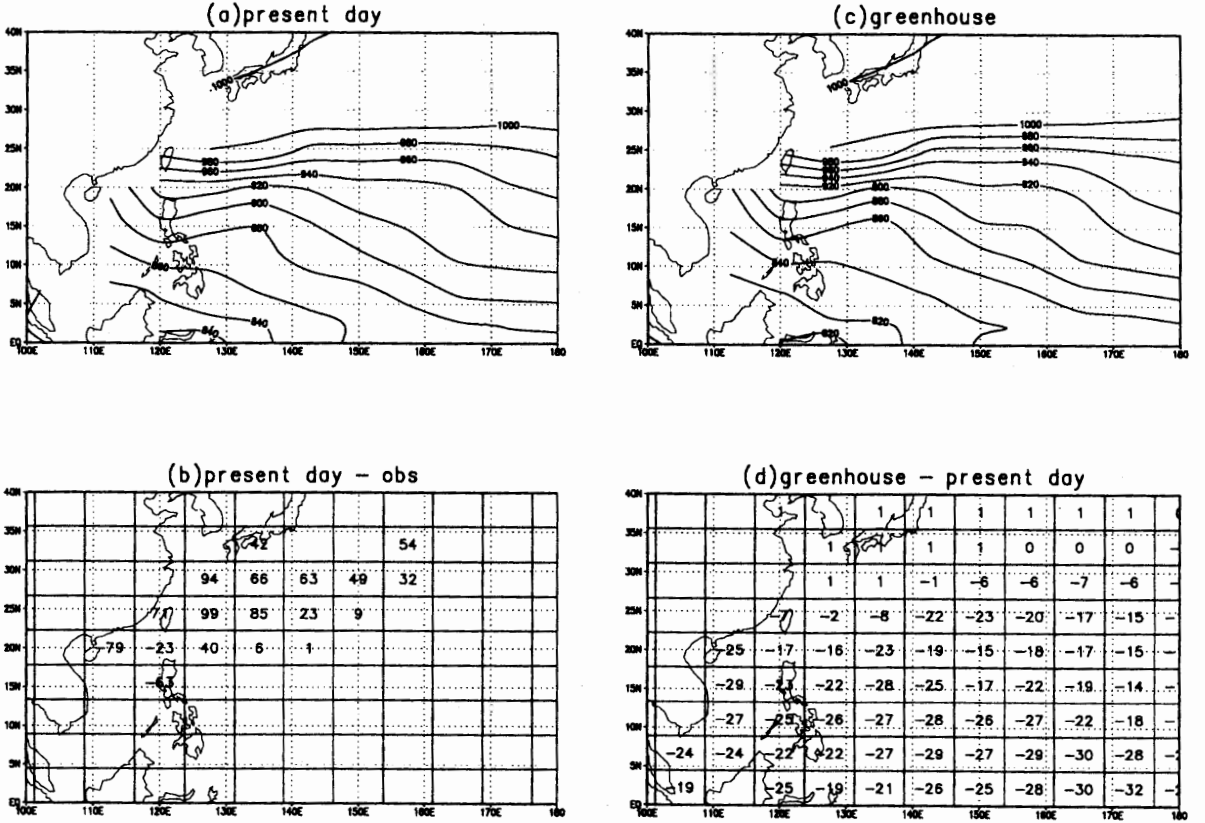

Figure 17.17 (a) Simulated maximum potential intensity (Holland model) for tropical cyclones in the north west Pacific from present-day climate simulations with the CCM1 for August; (b) differences (GCM simulations — observed) at GCM grid locations; (c) simulations of maximum potential intensity for a greenhouse-warmed climate; (d) differences ($2 \times CO_2$ GCM simulations — current GCM simulations).

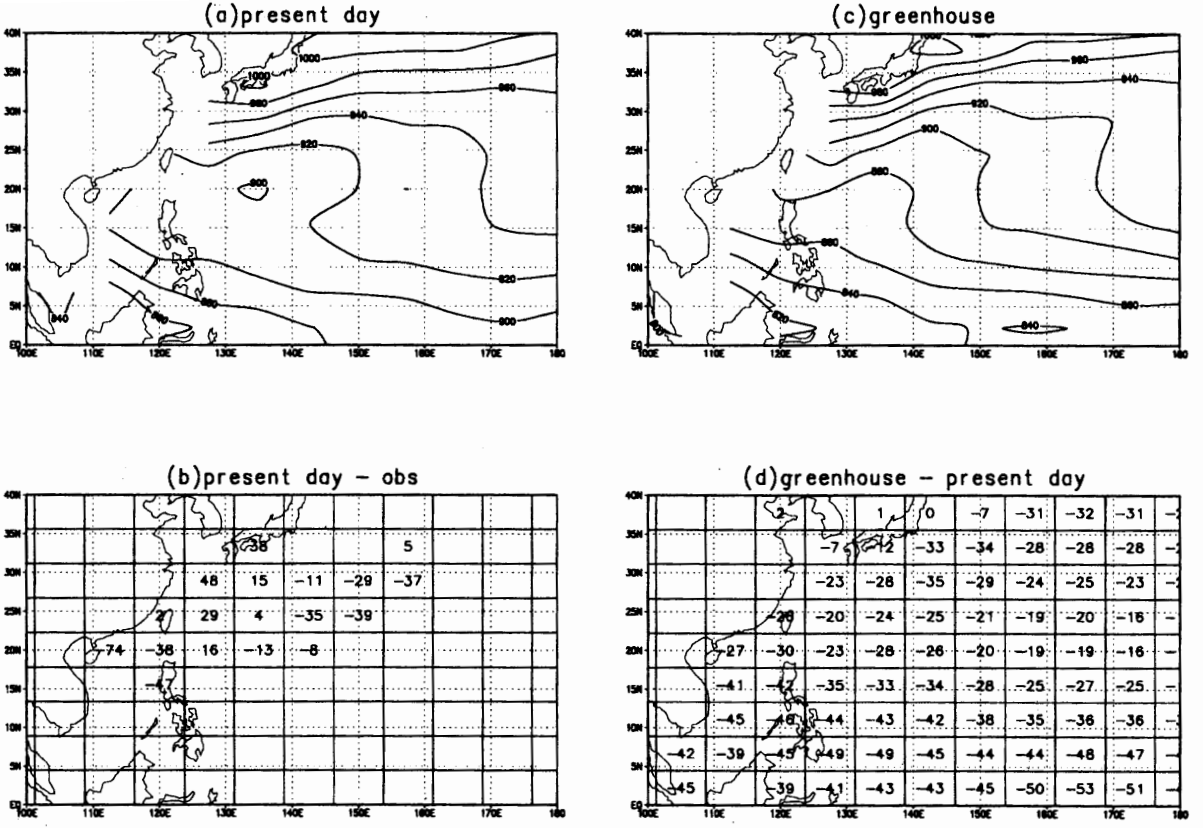

Figure 17.18 (a) Simulated maximum potential intensity (Holland model) for tropical cyclones in the north west Pacific from present-day climate simulations with the CCM1W for August; (b) differences (GCM simulations — observed) at GCM grid locations; (c) simulations of maximum potential intensity for a greenhouse-warmed climate; (d) differences ($2 \times CO_2$ GCM simulations — current GCM simulations).

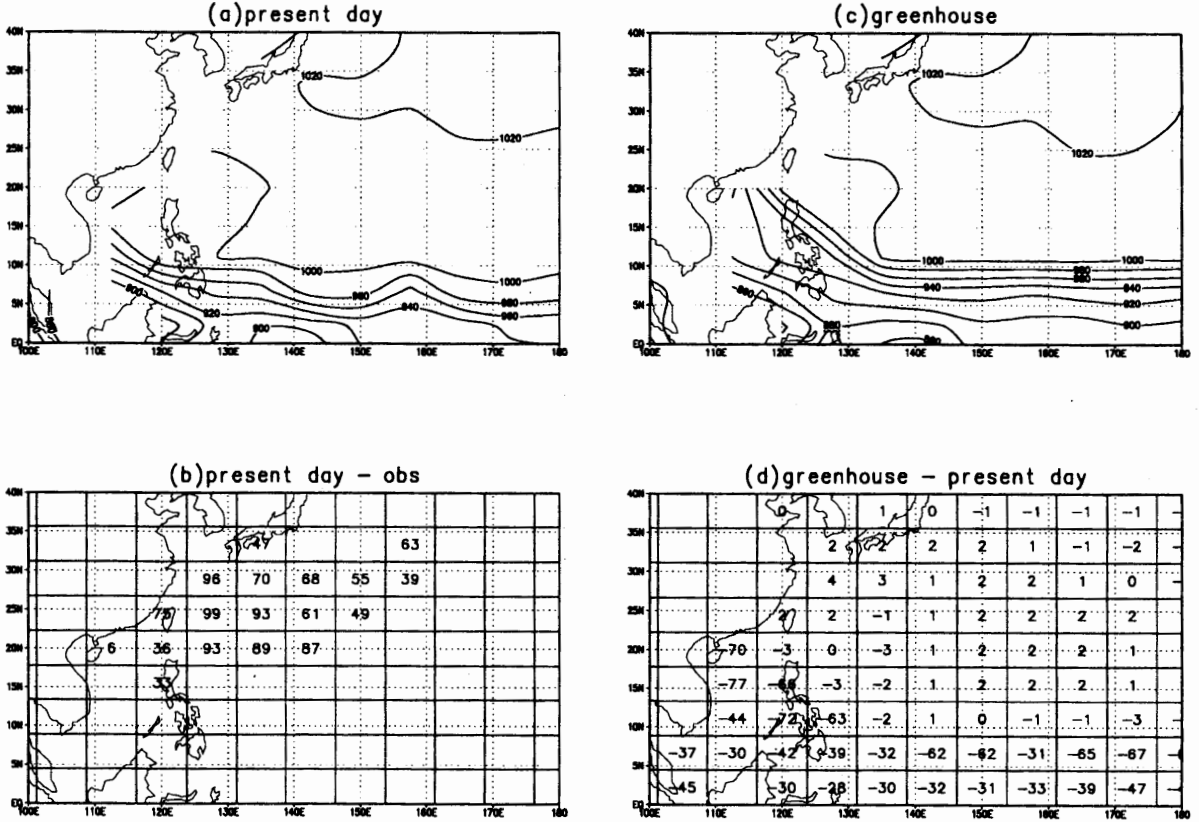

Figure 17.19 (a) Simulated maximum potential intensity (Holland model) for tropical cyclones in the north west Pacific from present-day climate simulations with the CCM0 for August; (b) differences (GCM simulations — observed) at GCM grid locations; (c) simulations of maximum potential intensity for a greenhouse-warmed climate; (d) differences ($2 \times CO_2$ GCM simulations — current GCM simulations).

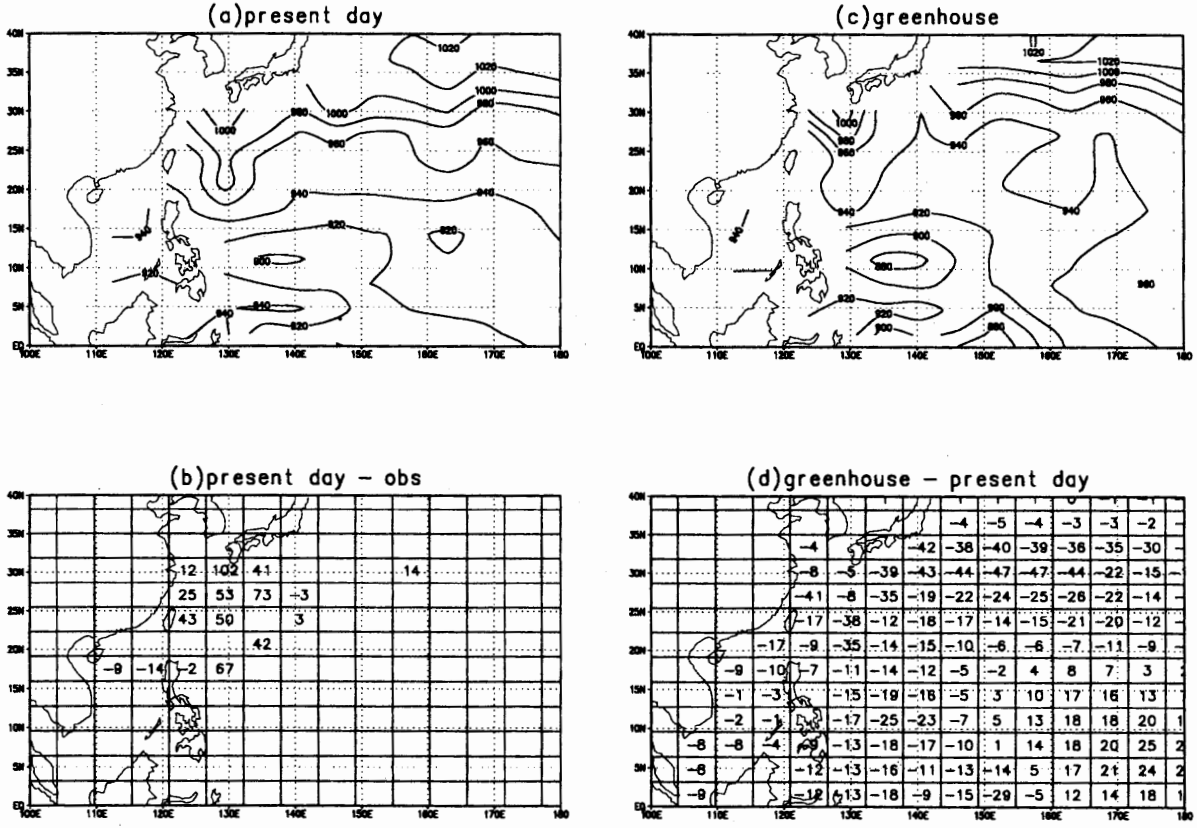

Figure 17.20 (a) Simulated maximum potential intensity (Holland model) for tropical cyclones in the north west Pacific from present-day climate simulations with the BMRC for August; (b) differences (GCM simulations — observed) at GCM grid locations; (c) simulations of maximum potential intensity for a greenhouse-warmed climate; (d) differences ($2 \times CO_2$ GCM simulations — current GCM simulations). (This GCM has a higher spatial resolution than the others so that more grid locations are displayed in part (b)).

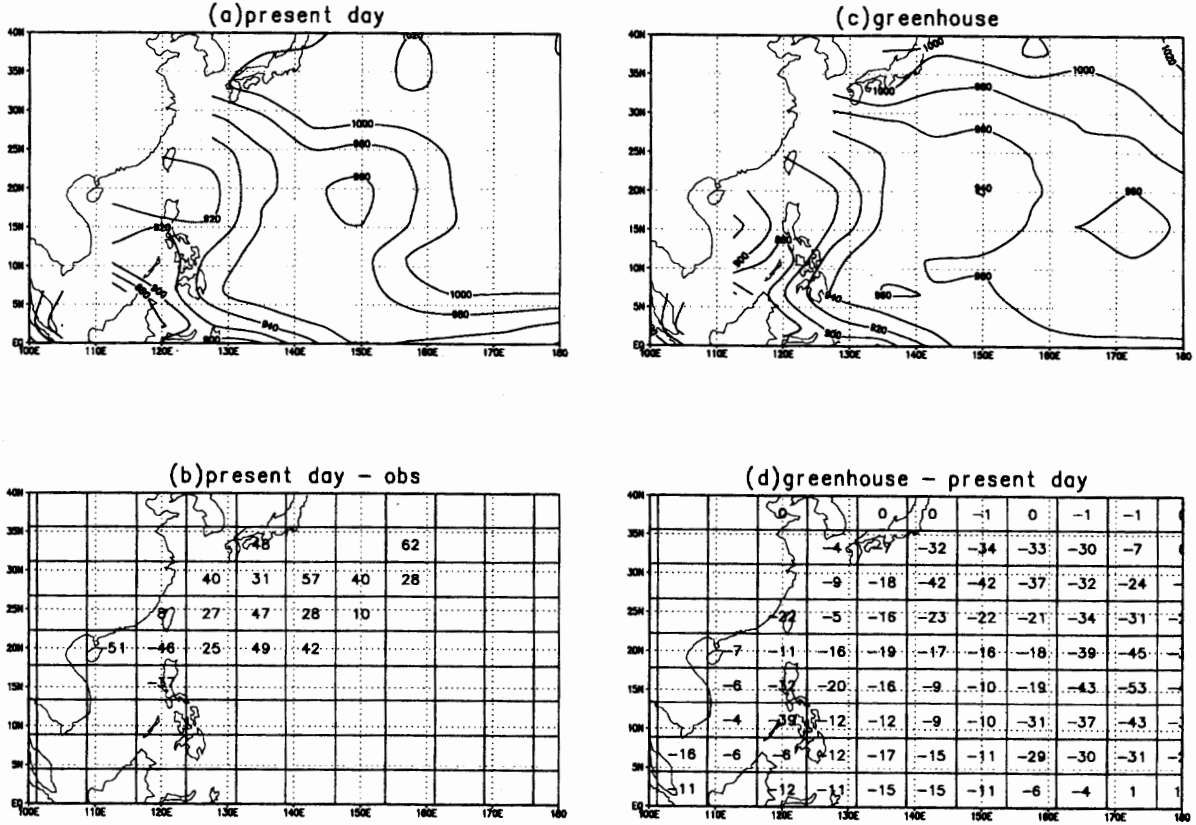

Figure 17.21 (a) Simulated maximum potential intensity (Holland model) for tropical cyclones in the north west Pacific from present-day climate simulations with the GENESIS for August; (b) differences (GCM simulations — observed) at GCM grid locations; (c) simulations of maximum potential intensity for a greenhouse-warmed climate; (d) differences ($2 \times CO_2$ GCM simulations — current GCM simulations).

The six MECCA models include five GCMs from NCAR and one GCM from BMRC. Each climate model includes a 50 m deep mixed ocean layer. The horizontal resolution of five of the GCM models is 7.5 degrees latitude by 4.5 degrees longitude (i.e. 48 × 40 grid points globally) while the BMRC model has a higher resolution of 64 × 56 grid points. Among the six models, CCM1-OZ, CCM1, CCM1W and GENESIS have 12 levels in the vertical, and CCM0 and BMRC have nine levels. The model simulations employed in the study are averaged over the last 10 years except for GENESIS where only five years of results were archived for analysis.

Figures 17.16–17.21 show the MPI results for each climate model. In each case, we indicate the MPI for current climatic conditions, the difference between simulated and observed MPI, obtained from the data sets described above, the predicted climatic MPIs, and the changes from current climate. Each grid square indicates the resolution of the climate model and only those grid squares with more than three cyclone observations were included in the analysis. We note that all thermodynamic models over estimate potential intensity in equatorial regions, where the dynamics are not able to support cyclone development (e.g. Gray 1968). For this reason, the region between the equator and 10°N is not analysed.

For CCM1-OZ (Figure 17.16), the model overpredicts MPI throughout most of the basin. We note that some overprediction is expected, because the maximum possible cyclone may not have been observed over the relatively short period of cyclone observations. Nevertheless, this model considerably overestimates MPI. The climatic changes in MPI are predicted to be a modest reduction of 20–30 hPa in central pressure, which is a fraction of the errors in the current climate assessment.

The MPI errors for CCM1 (Figure 17.17) vary from –79 hPa in the South China Sea to 99 hPa south of Japan. However, this model simulates generally weaker MPI for current climate than is observed, and substantially weaker than CCM1-OZ. Only modest MPI changes are predicted for a greenhouse climate.

The MPI distribution of CCM1W (Figure 17.18) contains a consistent error variation from negative in the south and east to positive in the north west. Errors range from –74 to 48 hPa, which is less than that for the previous two models. Predicted climate changes are modest, ranging from –46 to 1 hPa.

CCM0 produces very weak tropical cyclone MPI (Figure 17.19) for the current climate, with an error range of 6–99 hPa. The predicted climate changes are also modest, ranging from –77 to 4 hPa.

The BMRC model (Figure 17.20) has an error distribution ranging from –14 to 102 hPa. Interestingly, this model predicts weaker cyclones in some parts of the domain for a greenhouse climate.

The GENESIS model simulates generally weaker than observed MPI (Figure 17.21), except in the South China Sea. Predicted changes of MPI are similar to other models and range from –53 to 0 hPa.

17.5 Summary

This preliminary analysis indicates that thermodynamic models of tropical cyclone MPI are in relatively good agreement with available observations. The main differences are that the model MPIs are often more intense than observed, but this is at least partially explained by the relatively short period of observations. Application of the Holland model to MECCA climate models indicates that substantial errors occur in estimating current climatic conditions. These are mostly due to errors in SST. The models consistently predict a modest increase of around 20 hPa in MPI, with the exception of the BMRC model which predicts a weakening for part of the domain. Care needs to be taken with the application of this prediction, however, as the changes are much smaller than the errors in simulating the current climate.

Acknowledgments

This paper is CIC contribution number 95/41.

References

Abdullah, A.J. (1954) A proposed mechanism for the development of the eye of a hurricane. *Journal of Meteorology*, **11**, 189–195.

Bengtsson, L., Botzet, M. and Esch, M. (1994a) Hurricane-type vortices in a general circulation model, Part I. Max-Planck-Institut fur Meteorologie, Report No. 123.

Bengtsson, L., Botzet, M. and Esch, M. (1994b) Will greenhouse gas-induced warming over the next 50 years lead to higher frequency and greater intensity of hurricanes? Max-Planck-Institut fur Meteorologie, Report No. 139.

Broccoli, A.J. and Manabe, S. (1990) Can existing climate models be used to study anthropogenic changes in tropical cyclone climate? *Geophysical Research Letters*, **17**(11), 1917–1920.

Byers, R.H. (1944) *General Meteorology*, 2nd Ed., p. 645. New York: McGraw-Hill Book Company.

Dong, K. and Holland, G.J. (1994) A global view of the relationship between ENSO and tropical cyclone frequencies. *Acta Meteorology Sinica*, **8**, 19–29.

Demaria, M. and Kaplan, J. (1994) Sea surface temperature and the maximum intensity of Atlantic tropical cyclones. *Journal of Climate*, **7**, 1324–1334.

Dvorak, V.F. (1975) Tropical cyclone intensity analysis and forecasting from satellite imagery. *Monthly Weather Review*, **103**, 420–430.

Emanuel, K.A. (1987) The dependence of hurricane intensity on climate. *Nature*, **326**, 483–485.

Emanuel, K.A. (1988) The maximum intensity of hurricanes. *Journal of the Atmospheric Sciences*, **45**(7), 1143–1155.

Emanuel, K.A. (1991) The theory of hurricanes. *Annual Review in Fluid Mechanics*, **23**, 179–196.

Evans, J. (1993) Sensitivity of tropical cyclone intensity to sea surface temperature. *Journal of Climate*, **6**, 1133–1140.

Fairall, C.W., Kepert, J.D. and Holland, G.J. (1994) The effect of sea spray on surface energy transports over the ocean. *The Atmosphere Ocean System*, **2**, 121–142.

Gray, W.M. (1968) Global view of the origin of tropical disturbances and storms. *Monthly Weather Review*, **96**, 669–700.

Gray, W.M. (1975) Tropical cyclone genesis. Department of Atmospheric Science, Paper No. 232, Colorado State University, Ft. Collins, CO, p. 121.

Gray, W.M. (1979) Hurricanes: Their formation, structure and likely role in the tropical circulation. In *Meteorology over the Tropical Oceans*, edited by D.B. Shaw, pp. 278. Bracknell: Royal Meteorological Society.

Gray, W.M. (1984) Atlantic seasonal hurricane frequency: Part I: El Niño and 30mb quasi-biennial oscillation influences. *Monthly Weather Review*, **112**, 1649–1668.

Gray, W.M. and Landsea, C.W. (1992) African rainfall as a precursor of hurricane-related destruction on the US East Coast. *Bulletin of the American Meteorological Society*, **73**, 1352–1364.

Gray, W.M., Landsea, C.W., Mielke, P.W. Jnr. and Berry, K.J. (1993) Predicting Atlantic seasonal tropical cyclone activity by 1 August. *Weather Forecasting*, **8**, 73–86.

Gray, W.M., Landsea, C.W., Mielke, P.W. Jnr. and Berry, K.J. (1994) Predicting Atlantic seasonal tropical cyclone activity by 1 June. *Weather Forecasting*, **9**, 103–115.

Haarsma, R.J., Mitchell, J.F.B. and Senior, C.A. (1993) Tropical disturbance in a GCM. *Climate Dynamics*, **8**, 247–257.

Hirakuchi, H. and Giorgi, F. (unpub.) Multi-year present day and $2\times CO_2$ simulations of monsoon climate over eastern Asia and Japan with a regional climate model nested in a GCM.

Henderson-Sellers, A., Howe, W. and McGuffie, K. (1995) The MECCA analysis project. Special issue of *Global and Planetary Change*, **10**(1–4), 3–21.

Henderson-Sellers, A. (1996) Adaptation to climatic change: Its future role in Oceania. In *Greenhouse, coping with climate change*, edited by W.J. Bouma, G.I. Pearman and M. Manning, p. 349–376. Collingwood: CSIRO Publications.

Holland, G.J. (1981) On the quality of the Australian tropical cyclone data base. *Australian Meteorological Magazine*, **29**, 169–181.

Holland, G.J. (forthcoming) The maximum potential intensity of tropical cyclones. *Journal of Atmospheric Sciences*.

Kleinschmidt, E. Jnr. (1951) Principals of the theory of tropical cyclones. *Archives of the Materials of Geophysical Bicklimatology*, **4a**, 53–72.

Lighthill, J., Holland, G.J., Gray, W.M., Landsea, C.W., Craig, G., Evans, J., Kurihara, Y. and Guard, C. (1994) Global climate change and tropical cyclones. *Bulletin of the American Meteorological Society*, **75**(11), 2147–2157.

Maher, J.V. and Lee, D.M. (1977) Upper air statistics, Australia: Surface to 5 hPa, 1957 to 1975, pp. 202. Canberra: Australian Government Publishing Service.

Malkus, J.S. and Riehl, H. (1960) On the dynamics and energy transformations in steady-state Hurricanes. *Tellus*, **12**(1), 1–20.

Merrill, R.T. (1987) An experiment in statistical prediction of tropical cyclone intensity change. NOAA Technical Memo, NWS NHS-34, pp. 34.

Miller, B.I. (1958) On the maximum intensity of hurricanes. *Journal of Meteorology*, **15**, 184–195.

National Climate Data Center (1994a) Global Tropical and Extratropical Cyclone Climatic Atlas (GTECCA), Version 1, March 1994.

National Climate Data Center (1994b) Monthly Climatic Data for the World, April 1993, Vol. 46, No. 4.

Palmen, E. (1948) On the formation and structure of tropical hurricanes. *Geophysica*, **3**, 26–38.

Pudov, V.D. and Holland, G.J. (1994) Typhoons and oceans: Results of experimental investigations. BMRC Research Report No. 45. Melbourne: Bureau of Meteorology.

Riehl, H. (1954) *Tropical Meteorology*. New York: McGraw-Hill Book Company.

Ryan, B.F., Watterson, I.G. and Evans, J.L. (1992) Tropical cyclone frequencies inferred from Gray's yearly genesis parameter: Validation of GCM tropical climates. *Geophysical Research Letters*, **19**(18), 1831–1834.

Shay, J.K., Black, P.G., Mariano, A.J., Hawkins, J.D. and Elsberry, R.L. (1992) Upper ocean response to Hurricane Gilbert. *Journal of Geophysical Research*, **97**, 20227–20248.

Slutz, R.J., Lubker, S.J., Hiscox, J.D., Woodruff, S.D., Jenne, R.L., Joseph, D.H., Steurer, P.M. and Elms, J.D. (1985) COADS Comprehensive Ocean-Atmosphere Data Set. Release 1. Boulder, CO: Climate Research Program, Environmental Research Laboratories.